Chem

CellPress

Article

# Sculpting photoproducts with DNA origami

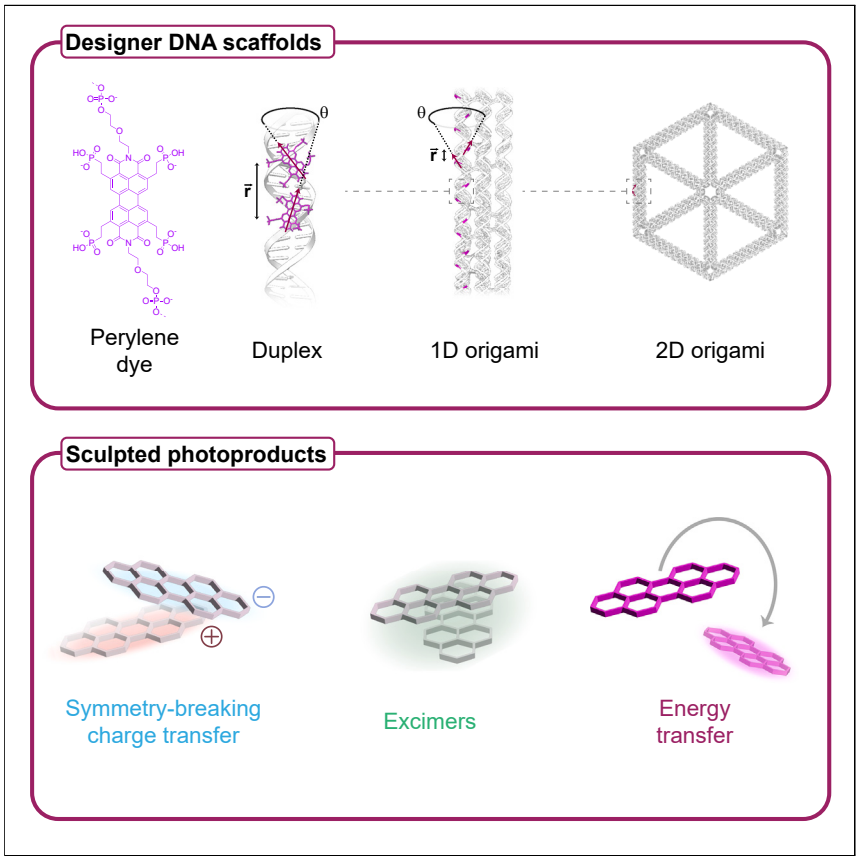


Excitonic systems depend sensitively on intermolecular couplings between constituent dyes, which are a function of their distances and relative orientations. Here, we developed a high-throughput platform to program couplings using DNA origami and tailored dye-oligonucleotide synthesis. We used ultrafast spectroscopy, electron microscopy, and molecular dynamics simulations to characterize the sculpted excitonic photoproducts. Leveraging the programmability and rigidity of DNA origami, these systems can be designed for a wide range of functionality, including excimer formation, charge transfer, and exciton transport.

Jeffrey Gorman, Stephanie M. Hart, Torsten John, ..., Adam P. Willard, Gabriela S. Schlau-Cohen, Mark Bathe

awillard@mit.edu (A.P.W.)
gssc@mit.edu (G.S.S.-C.)
mark.bathe@mit.edu (M.B.)

## Highlights

DNA origami is used to program PDI couplings through nanoscale dye positioning

Synthetic photochemical machinery containing 20+ dyes is realized

Charge transfer, exciton transport, and excimer formation are selectively programmed

Gorman et al., Chem *10*, 1553–1575
May 9, 2024 
https://doi.org/10.1016/j.chempr.2024.03.007

Chem

CellPress

Article

# Sculpting photoproducts with DNA origami

Jeffrey Gorman,[1,5] Stephanie M. Hart,[2,5] Torsten John,[1,3] Maria A. Castellanos,[2] Dvir Harris,[2] Molly F. Parsons,[1] James L. Banal,[1] Adam P. Willard,[2,*] Gabriela S. Schlau-Cohen,[2,*] and Mark Bathe[1,4,*]

## SUMMARY

**Natural light-harvesting systems spatially organize densely packed dyes in different configurations to either transport excitons or convert them into charged photoproducts, with high efficiency. In contrast, artificial photosystems like organic solar cells and light-emitting diodes lack this fine structural control, limiting their efficiency. Thus, biomimetic multi-dye systems are needed to organize dyes with the sub-nanometer spatial control required to "sculpt" resulting photoproducts. Here, we synthesize 11 distinct perylene diimide (PDI) dimers integrated into DNA origami nanostructures and identify dimer architectures that offer discrete control over exciton transport versus charge separation. The large structural space and site tunability of origami uniquely provide controlled PDI dimer packing to form distinct excimer photoproducts that are sensitive to interdye configurations. In the future, this platform will enable large-scale programmed assembly of dyes mimicking natural systems to sculpt distinct photophysical products needed for a broad range of optoelectronic devices, including solar energy converters and quantum information processors.**

## INTRODUCTION

The functions of photovoltaics, light-emitting diodes, and photochemical reactions broadly rely on a myriad of photoinduced product states, which generate outcomes including photons,[1,2] heat,[3–6] or charge-separated excited states.[7,8] In dye-based systems, these product states often leverage delocalized excited states, called excitons,[1,8–56] which evolve into product states selected through the nature of interdye coupling. For example, exciton transport is driven by long-range dipolar coupling, whereas exciton evolution into free charges for photochemical conversion is realized by shorter-range, charge-transfer (CT) coupling. Importantly, subtle structural changes within optically active materials can result in entirely distinct photophysical products.

In photosynthesis, nature converts light into chemical fuel by spatially organizing interdye couplings using a protein environment. Mimicking nature's ability to select for either exciton transport or CT via a local multi-dye structure offers the potential to unlock new design principles for organic solar cells. For example, organic systems could absorb, collect, and split excitons using the same dye moiety via symmetry-breakking CT (SBCT) and minimize energy loss and recombination.[57,58] However, these devices and their pre-specified product states require precise control over the spatial positioning and resultant coupling between numerous dyes.[59]

A number of synthetic strategies have attempted to realize high efficiency artificial light harvesting through multi-dye positional control. Simple, covalent dimers can

## THE BIGGER PICTURE

Enhancing the efficiency of solar light harvesting and electronics is essential to reducing our carbon footprint. Effectively managing excitons, the carriers of electronic energy at the molecular scale, is central to this mission. Sculpting the fate of excitons, whether transforming into charges or high spin states, depends sensitively on the spatial organization of the constituent molecular dyes. Although natural photosynthetic systems control dye coupling with protein scaffolds, synthetically replicating the structural precision of proteins has been a long-standing challenge. In this study, we used self-assembled DNA as the control medium for synthetic dye molecules to generate desired excitonic photoproducts. This pre-programmed precision establishes a foundation for tailored dye interactions, enhancing functionality for excitonic computing, sensing, and biomimetic light-harvesting assemblies.

  

be used to alter interdye coupling to select for product states.[58–64] However, matching the size and variability realized by natural protein-pigment complexes using covalent chemistry is impractical, considering their low solubility, low synthetic yield, and limited structural control.[61,65] The larger scale of natural systems has been achieved with polymers, which can support multiple dyes along their flexible backbone,[12–20,66,67] or amphiphilic dyes, which can self-assemble to produce extended aggregates.[21–26] However, both approaches suffer from polydispersity in the resulting multi-dye assemblies. Alternatively, metal- or covalent-organic frameworks (MOFs/COFs) can enable well-defined sub-nm scale dye arrays[27,28] but are confined to specific geometries that limit the range of available couplings. Finally, proteins can provide a "scaffold" for non-uniform arrays,[29–31] but dye addition typically occurs after protein folding, which restricts the accessible locations and number of sites. Thus, robust synthetic strategies for the interdye distances and couplings needed to replicate the function of natural-light-harvesting systems remain an outstanding challenge.

Nucleic acid nanotechnology offers the synthetic capability to orchestrate the spatial arrangement of molecules within hybridized DNA sequences, including dye dipole orientational control, using predictable Watson-Crick base pairing.[32,33] Incorporating perylene diimides (PDIs) into DNA sequences could offer the spatial control over multi-dye organization and, therefore, couplings needed to generate charges, excimers, and other product states via rational design. Numerous studies have demonstrated the effectiveness of using DNA for multi-dye assembly,[34–49] including strongly coupled dyes that undergo exciton evolution.[50–56,68–76] However, the incorporation of multiple dyes can destabilize the DNA duplex by disrupting base pairing. To address this, multi-duplex[34,77–81] and higher rigidity DNA motifs[74,75,82–84] have been explored that distribute dyes across numerous duplexes, including with DNA origami.[85–94] However, these reports have mostly focused on commercial dyes that lack the energetics needed for CT.

PDIs represent one exemplary class of promising dyes that can access numerous product states, including SBCT, excimers, and others.[58,95–98] However, control over their distinct product states has been hampered by the inability to program PDIs into different, specific structures and their resulting couplings.[60–62] For example, cofacial, slip-stacked PDI dimers mediate SBCT through enhanced CT coupling,[58,99] whereas highly rotated dimers form excimers.[100,101] Despite their utility, synthetic approaches broadly remain limited in their control over multi-dye organizations of PDIs, tetracenes, diketopyrrolopyrroles, etc.,[59,72,102] which is needed to program distinct photoproducts.

Here, we achieve spatial control over distinct exciton product states by templating PDIs on DNA origami (Figure 1). Toward this end, we leverage programmable DNA synthesis to identify three specific, functional dimer architectures: a strongly coupled SBCT-active slip stack, an energy-transfer-active non-cofacial system, and an excimer-active rotated dimer system. Combining time-resolved spectroscopy with molecular dynamics (MD) and quantum chemical calculations, we find that DNA synthesis with single-nucleotide (nt) precision can be exploited to shift CT-mediated photoproducts, namely to sculpt photoproducts by structural reorganization of PDI dimers in a more rapid and straightforward manner than can be achieved using covalent strategies. This work offers a pathway for high-throughput screening of DNA origami templated dye assemblies to discover excited-state evolution via rationally designed multi-dye scaffolding, enabling the precise installation of controlled dyes and their photoproducts. Selective control over CT coupling

[1]Department of Biological Engineering, Massachusetts Institute of Technology, Cambridge, MA 02139, USA

[2]Department of Chemistry, Massachusetts Institute of Technology, Cambridge, MA 02139, USA

[3]Present address: Max Planck Institute for Polymer Research, Ackermannweg 10, 55128 Mainz, Germany

[4]Lead contact

[5]These authors contributed equally

*Correspondence: awillard@mit.edu (A.P.W.), gssc@mit.edu (G.S.S.-C.), mark.bathe@mit.edu (M.B.)

https://doi.org/10.1016/j.chempr.2024.03.007

CellPress

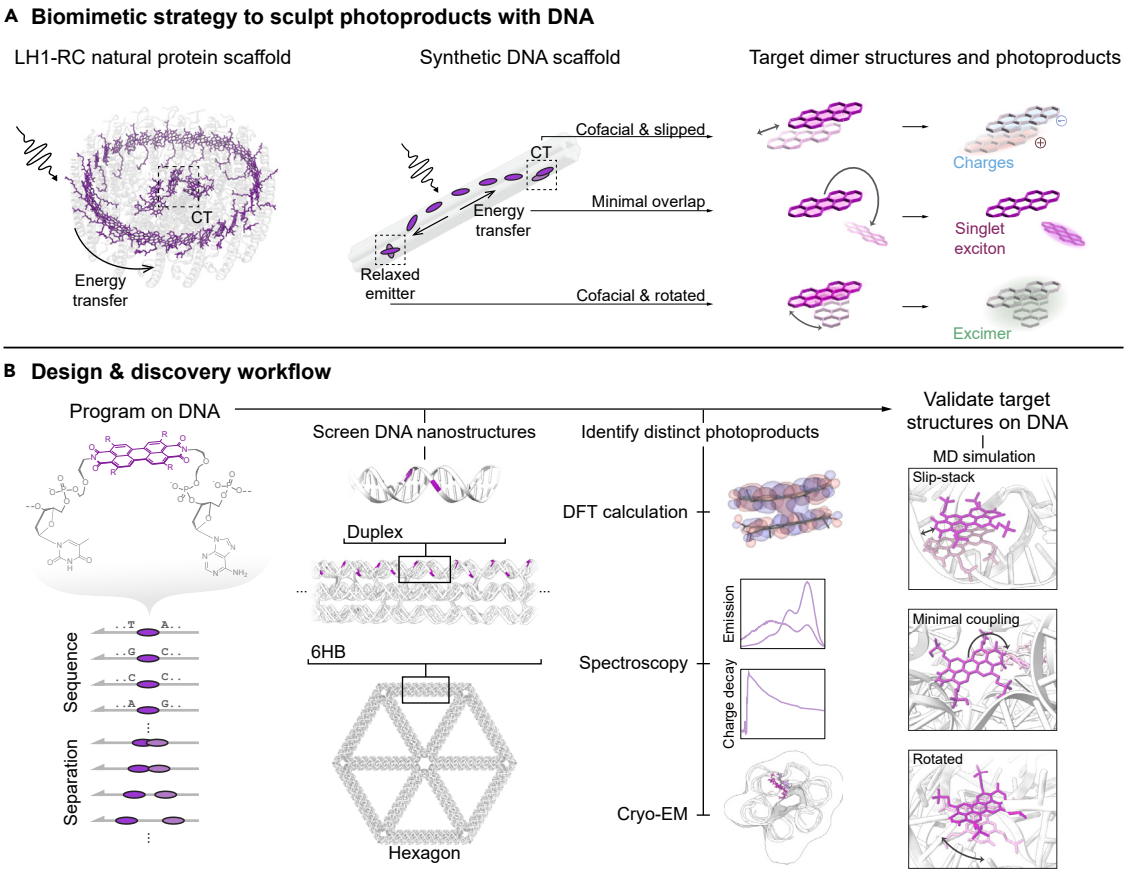


**Figure 1. Schematic overview and workflow**

(A) In the light-harvesting complex 1 reaction center (LH1-RC),[103] the bacteriochlorophyll dyes (purple) assemble into a dense ring structure organized by the protein scaffold (gray). Outer dyes are optimized for energy transfer, while the central reaction center form charges by charge transfer (CT). Our bio-inspired DNA nanotechnology approach aims to self-assemble perylene diimide (PDI) dimers (purple) on a DNA origami (gray), which similarly forms charges by CT, energy transfer by weakly coupled dyes, and strongly coupled excimers. Cartoons of required dimer structures for these photoproducts are shown.

(B) Synthetic design and photoproduct discovery in this work. We installed multiple PDIs in a DNA sequence library that were assembled in DNA duplexes, six-helix bundles (6HBs), and hexagonal origami. This enables precise, programmed, and multivalent dye positions. The DNA library was screened by molecular dynamics (MD) simulations and density functional theory (DFT) calculations, spectroscopy, and cryogenic electron microscopy (cryo-EM). Library members that yielded photoproduct hits were modeled by MD, and we found that optimal PDI dimer geometries were replicated on these DNA origami structures.

provides an attractive platform, integrating both exciton and CT design for advanced excitonic circuits in synthetic light-harvesting systems.

## RESULTS

### Design of origami-compatible PDIs

Although PDI-DNA conjugate synthesis has been demonstrated previously,[52,104–110] hydrophobicity in those studies led to uncontrolled aggregation. To address this, we targeted a hydrophilic PDI via four ortho-ethylphosphonate groups[111] that were compatible with single-stranded DNA (ssDNA) synthesis (Figure 2A).[112] Ortho-functionalization has been implicated in slip-stacked PDI dimers, which we identified as a target structure for SBCT.[58,98] Finding that the DNA-free dye analog yielded a non-aggregating PDI in water (Figure S1), we next redesigned the dye (Figure S2) for insertion into the phosphodiester backbone of ssDNA (Figure 2A) by using solid-phase oligonucleotide synthesis (SPOS).

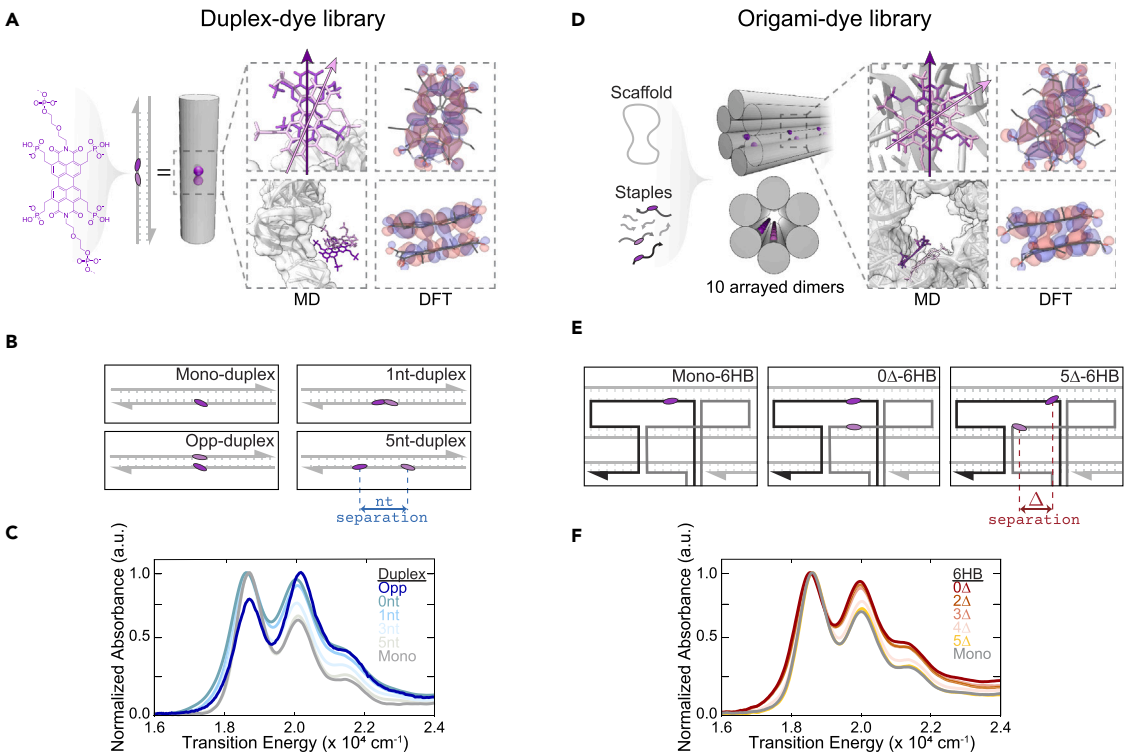


**Figure 2. Assembling PDI on duplex and origami array platforms**

(A) Duplex DNA schematic with PDI inserted in the backbone (purple). Inset: representative molecular dynamics (MD) structures with highlighted transition dipoles and highest occupied molecular orbital diagrams by density functional theory (DFT).

(B) Electronic coupling is programmed by varying the base sequence separation across different structures. In duplexes, PDIs are separated on the same (*n* nt-duplex) or opposite strands (opp-duplex) by predefined nucleotide spacing.

(C) Peak-normalized steady-state absorption of PDIs in duplexes showing greater electronic coupling with shorter nucleotide separation.

(D) Origami array schematic with PDI insertion. Each six-helix bundle (6HB) rod-like array is assembled in a one-pot reaction that includes 20 unique, abiotic PDI-labeled staple strands. The resulting 6HB origami contains 10 repeat units, each containing a PDI dimer (purple dots) in the cavity. Inset: representative MD structure of a single dimer, with transition dipoles highlighted, and highest occupied molecular orbital diagrams.

(E) Select 2D strand routing. PDI dimers are tuned by their base-pair separation *n*Δ encoded in the PDI-staple nucleotide sequences over multiple duplexes. For each 6HB, all 10 PDI dimer staple positions are simultaneously tuned. For clarity, only 3 local helices are shown.

(F) Peak-normalized steady-state absorption of PDIs in origami showing greater electronic coupling with shorter nucleotide separation.

To confirm that our PDI-DNA assembly could control aggregation, we first built monomer constructs (mono-duplex) generated by structuring a single PDI within ssDNA, hybridized with a complementary non-dye-containing ssDNA that should yield no excitonic coupling (Figure 2B). PDI strands efficiently formed duplexes by gel analysis (Figure S3). To track the effectiveness of our control, the relative excitonic coupling of the mono-duplex was analyzed using steady-state absorbance (Figure 2C). Reproduction of the natural vibronic progression of a PDI monomer, specifically 0–0 (18,655 $cm^{-1}$) and 0–1 (20,050 $cm^{-1}$), arising from coupling of the electronic transition to the 1,400-$cm^{-1}$ symmetric vinyl stretching mode,[113,114] suggested that the *ortho* phosphonate groups of the PDI did not alter its electronic structure significantly, in contrast to bay-modified PDIs.[115] This negative control showed a vibronic progression that is typical of an unaggregated PDI. This result confirmed that our PDI derivatives could only be aggregated in a controllable fashion, without off-target hydrophobicity-induced excitonic coupling.

## Controlling PDI coupling with DNA templating

Having established that a single PDI could be programmed, we next sought to extend and test our ability to organize dimers. We rationally controlled the positions

of PDIs within each ssDNA and its local DNA sequence by using SPOS (Figure 2B). The first configuration templated PDI dimers on opposite sides of the DNA duplex (opp-duplex), similar to previous work.[106,110,116] The second configuration templated two PDIs consecutively (0 nt duplex) or separated by 1-, 3-, or 5-nt spacers (1 nt duplex, 3 nt duplex, or 5 nt duplex, respectively) along the same ssDNA and hybridized to form the double-stranded DNA (dsDNA) duplex (Figure 2C). Nt-controlled spacings are particularly attractive, as SPOS produce sequence variants in parallel.[72,73] We annealed each strand with its complement to produce a library of duplexes to explore multiple dimer configurations that could mimic the target slip-stacked and twisted dimer conformations.

To validate our predefined PDI dimer control, we analyzed the absorbance spectra of all PDI dimers, as any changes would provide clear signatures consistent with excitonic coupling. Previous work showed that the PDI vibronic peak ratio directly reports on coupling strength.[58,60,61,63,99,102,117–120] In all dimers described in our work, the oscillator strength of the 0–0 vibronic band was redistributed to the 0–1 band, which is a spectroscopic signature characteristic of cofacial aggregates, also referred to as an H-like aggregate structure.[102,118] The opp-duplex construct exhibited the strongest excitonic coupling, as observed in its high 0–1/0–0 ratio (∼2-fold increase relative to the monomer) compared with the consecutive PDI dimers on the same strand in the 0 nt duplex (∼1.5-fold increase relative to the monomer; Figure 2C). Larger inversion of vibronic peaks has commonly been ascribed to greater orbital overlap between cofacially assembled PDIs in aggregates.[121] The nt-spaced constructs showed recovery of the 0–1 and 0–0 vibronic band intensities of the monomer as the number of nt spacers increased, with full recovery of the vibronic bands achieved using 5-nt spacers. Unlike our previous work on zwitterionic-modified duplex constructs,[73] these results suggest that the DNA duplex can overcome the stacking energy of the modified PDI dimers and that inter-construct aggregation, as observed in unmodified duplex-bound PDIs, does not occur here.[104,110] Our results show that phosphonate-PDI derivatives are good candidates for programmed PDI excitonic coupling and ensure that coupling between PDIs is a function of DNA assembly only, not overpowered by dye hydrophobicity.

## DNA-origami-directed exciton coupling

Single duplex scaffolds are too small to organize tens to hundreds of dyes reliably, as multiple insertions can destabilize duplex stability.[37] Although multiple PDIs have been inserted into DNA, many of these still aggregate in "monomeric" systems or struggle to form extended assemblies.[52] To move toward larger biomimetic scales, we integrated these PDI assemblies into higher-order six-helix-bundle (6HB) DNA origami, with 20 PDIs per assembly (Figure 2D). To achieve this, we designed a set of ssDNA that repeated their self-assembled structure every 42 nts, i.e., every four complete turns of a dsDNA to retain a straight 6HB design (Figures S4–S10; Data S1).

6HBs are composed of six intertwined DNA helices to form a rigid cylinder,[32,33,122] reliably built using the DNA origami technique. In this approach, a long ssDNA scaffold is folded by many shorter, synthetic ssDNAs termed "staples," which are base-complementary to remote regions of the scaffold, effectively folding the system into a rigid cylinder. To explore the available PDI interactions and their photophysics, we used a series of PDI-dimer configurations in the larger available structural space of a 6HB to find intermolecular couplings that facilitated excimer formation and CT. We expected the 6HB motif to be a good choice for organic dye photophysics because its ∼2-nm inner cavity matches the limit of non-negligible excitonic coupling.[123]

Because DNA origami is typically queried in a relatively dilute solution (<1 μM), single PDI dimers per origami would be too sparse for spectroscopic investigations. To address this issue, we created an array of decoupled 10 dimers along a 6HB (Figure 2D). Within the current design construct, it is important to note that the scaffold sequence is essentially non-repeating, so that even though strand positions and crossovers of each repeat unit are nearly identical, the local base sequence varies between segments. For PDI placement, we selected positions to self-assemble after annealing onto the inner surface of the 6HB cavity (Figure 2D). For each construct, we selected rigid PDI positions across neighboring helices in the 6HB. This strategy was chosen so each helix only contained a single-nt substitution per PDI to maintain duplex stability. In addition, the PDI sites were located at the center of the staple sequences, far from their 5′ or 3′ staple termini, which are prone to local DNA melting/unwinding.[124] Increased PDI density meant <200 nM origami concentrations were required for all optical measurements, dilute enough to avoid gelation.[125,126]

Using these design elements to screen for long- and short-range excitonic coupling, we fabricated a series of DNA origami constructs with PDI dimers that were separated by up to 5 nts: 0Δ, 2Δ, 3Δ, 4Δ, and 5Δ-6HB. Here, the "Δ" nomenclature designated the base-pair (bp) separation between two PDIs along the long axis of the nanotube (Figure 2E). These distances were chosen to match those explored on duplexes. Additionally, neighboring helices in 6HBs twist away from one another, leading to larger pitching/angular separation of PDI dimers across two helices, with the 5Δ separation representing the furthest available distance before each dye is displayed on opposite sides of the 6HB cavity. As a control, we generated a mono-6HB containing 20 PDIs, with every PDI well-separated by ≥23 bps (∼8 nm) that should remain uncoupled if the coupling was solely DNA encoded.

To validate that the 6HB annealed and assembled correctly, we characterized constructs by agarose gel electrophoresis (AGE) and transmission electron microscopy (TEM). AGE revealed a gel band shift when comparing the unhybridized scaffold to the fully assembled origami mix across all samples, consistent with fully self-assembled origami (Figure S11). All 6HBs were assembled and purified in high yield >77% (Table S1). We achieved complete separation of low-molecular-weight excess staples in the crude mixture from the purified folded origami by using molecular-weight-cutoff spin filtration. TEM imaging revealed assembly of ∼150-nm rod-like structures, as expected, and PDI-modified 6HBs were essentially identical to the substituted 6HB analog by both AGE and TEM (Figures S11–S18).

To investigate whether inserting PDIs disrupted origami self-assembly, we interrogated the global melting temperature of the 6HBs, where a significant reduction in melting temperature would indicate that PDIs were inhibiting or limiting hybridization. Thermal melting curves confirmed structural stability in the sequence design, showing no change or destabilization between unlabeled-6HB and PDI-labeled 6HB constructs (Figure S19). In contrast, PDI-duplex structures were significantly destabilized by PDI insertion (Figure S20), highlighting the structural benefit of origami toward larger-scale dye assembly. Consistent with the target design, the mono-6HB control yielded a monomeric absorption spectrum indicative of non-aggregated PDIs (Figure 2F). PDI dimers 0–5Δ-6HB showed a redistribution of 0–0 and 0–1 oscillator strengths, with 0Δ-6HB and 2Δ-6HB constructs exhibiting the highest 0–1/0–0 vibronic intensity ratio (∼1.4-fold increase relative to the monomer). Notably, absorbance measurements of the unhybridized PDI-ssDNA staples, which comprised the dimers in the 6HB constructs, exhibited only monomeric absorbance spectra (Figure S21) across the same 100- to 500-nM concentration regime of the

origami studied here. This indicated that DNA origami scaffolds specifically templated the excitonic coupling observed by the PDI dimers.

In contrast to opp-duplex, the 0–1/0–0 vibronic intensity ratio of the 0Δ-6HB was lower, suggesting weaker excitonic coupling. However, the origin of the observed lower excitonic coupling may result from the complex interplay of excitonic and vibrational interactions in PDI dimers, which is highly sensitive to the relative displacement, angle, and distance between π-stacked PDIs, as described previously.[102,118,121] Further, as we observed previously for squaraines,[73] interference between long-range Coulombic and short-range CT interactions could also contribute to the differences in the excitonic coupling between the constructs.[117]

### Characterizing target PDI dimer structures on DNA

Although absorptive changes in aggregates indicate their coupling, to obtain a clearer picture of how PDIs might stack and the impact on exciton evolution, we performed all-atom MD simulations of 0Δ-, 2Δ-, and 4Δ-6HBs, and opp- and 0 nt-duplex structures, in triplicate (Figures S22–S31; Videos S1, S2, S3, S4, S5, S6, S7, S8, S9, S10, S11, S12, S13, S14, and S15). Specifically, we explored DNA designs that generated: slip-stacked PDI dimers, which we anticipated would yield SBCT; non-overlapping dimers, which we expected to support energy transfer; and rotated PDIs to form excimers. These simulations revealed a propensity for π-stacking across all simulated constructs, with center-of-mass (COM) distances between each dye yielding ∼4 Å, typical of aggregated PDIs.[127] We identified the 0 nt-duplex as an SBCT candidate because of its small 17° ± 5° rotational offset and slip-stacked packing configuration. We note, some MD replicates yielded interdye COM distances >1.4 nm (Figures S30 and S31) within the simulation time that were inconsistent with the strong excitonic coupling observed in their steady-state spectra in Figure 2C and were therefore discarded from our structural analysis. We speculate this may be a function of the very different starting geometries used in our simulations to avoid potential bias in the PDI temporal π-stacking assembly. Nonetheless, the observed disorder indicated a broad configuration space with multiple subpopulations of PDI dimers, a phenomenon that aligned with our time-resolved experiments, *vide infra*. For the larger 6HBs, simulations were performed using a single 42-bp repeat unit with a single PDI pair to exploit linearly repeating symmetry to reduce computational cost. This was contrasted with the 10 PDI pairs that were equally spaced across the one-dimensional (1D) origami rod in all wet experiments. Nevertheless, the 42-bp model still necessitated a sizable simulation box that constrained the overall simulation time. Once again, we noticed variations in MD replicate trajectories that we tentatively attributed to different PDI starting configurations influencing the pathway of π-stacking. We note that the observed heterogeneity in 0- and 2Δ-6HBs was considerably lower than in the duplexes, alluding to clear dimer subpopulations in these systems. Whereas no cofacial interactions were observed in 4Δ-6HB (COM > 14 Å) despite the close PDI placement within the sequence, the 0Δ-6HB construct achieved similarly stacked configurations, with a COM ≈ 4.7 Å. As expected, increasing base separation in the 2Δ-6HB construct reduced similar cofacial interactions (COM ≈ 5.5 Å). Although observed π-stacking distances were similar among 6HB and duplexes, 6HB structures yielded larger rotational offsets than their duplex counterparts. Hence, we anticipated excimers might emerge in these origami structures.

To compare the MD simulations with experiments, and validate whether we have control over where PDIs are displayed on the 6HB surface, we employed cryogenic electron microscopy (cryo-EM) to extract the PDI structure in the 6HB origami.

Cryo-EM required a higher concentration (>950 nM), which led to some aggregation of origami observed by AGE (Figure S11). However, we do not expect that aggregation impacted PDI photophysics, which were interrogated at considerably lower concentrations of ~250 nM, and given that any inter-origami PDI interactions would be >4 nm apart. Direct reconstruction of a single 1D rod-like PDI-6HB failed due to challenging image alignment of the symmetric object. To improve image alignment and reconstruction, we instead implemented a two-dimensional (2D) hexagonal honeycomb origami structure (Figures S32 and S33; Table S16; Data S2), which we previously found yielded cryo-EM reconstruction of up to 1.4 nm resolution.[128] We characterized the hexagonal origami in line with our PDI-6HBs, again observing aggregation by AGE in these high-concentration samples (Figures S34 and S35). We highlight, each edge of the hexagonal mesh is composed of a 6HB rod, interconnected by unhybridized strand vertices. To replicate the PDI environment described earlier in the 6HB rods, we swapped a single 0Δ-6HB PDI dimer into a spoke of the hexagonal origami, with the same PDI-labeled staple routing topology as described for the 1D 6HB-rod for all optical measurements in this work. To further improve image alignment, this hexagonal origami was augmented with a symmetry-breaking C1 handle. We elucidated the 0Δ-PDIs conformation within the 6HB edge via three-dimensional (3D) reconstruction (Figure S36). We observed local asymmetric density at the locus of the two PDIs on the origami, a result of the larger steric bulk and chemical size of the dyes compared with a single nt. To benchmark this, we used rigid-body fitting of a hexagonal origami model from a coarse-grained DNA model (oxDNA) MD simulations[129] to the cryo-EM density of the 0Δ-6HB, observing reasonable structural overlap where the PDIs were positioned. This result indicated that the two PDIs in 0Δ were displayed on the inside of the 6HB cavity, as initially designed and resulting from the MD simulations. Unfortunately, the cryo-EM resolution was not high enough to discern specific atomic features or infer dye orientations and distances. Moreover, cryo-EM analysis was impossible with single, small, and less globally rigid duplex structures, as is typical. We anticipate that improved origami design and reconstruction algorithms might in the future enable increased structural resolution together with unambiguous identification of dimer structures.

## Tracking excited-state properties in PDI-DNA origami

Excimer species can be identified by their distinct emission spectra (Figures 3A and 3B). The uncoupled mono-6HB control exhibited vibronically well-resolved emission peaks, mirror-imaged from its absorption spectra. However, 0–3Δ-6HB dimers yielded new, broader, featureless, and red-shifted emissive species. These spectra are typically assigned to H-type PDIs,[121] which may emit via their excimer state.[59,130,131] Although excimers have been reported in a number of polydisperse PDI structures,[52,104,110,132] these studied lacked the fine structural control offered by DNA origami. To quantify the extent of this excimer population and coupling, we decomposed the emission spectra into a two-state model of Frenkel exciton and excimer emission species (Figure 3C), plotted against approximate exciton coupling values ($J_{exp}$) extracted from the linear absorption spectra (Figure S37). We found that excimer population and exciton coupling were proportional to PDI separation (Δ) on the 6HB origami, consistent with significant interdye orbital overlap indicated by MD simulations. Excimers form as a result of excitonic coupling that splits the monomeric $S_1$ state into lower, dark (H-type) and upper, bright (J-type) energy levels.[133,134] Although H-type optical transitions are symmetry-forbidden, this selection rule is lifted in highly rotated excited PDIs, which yields this diagnostic emission.[100] The versatility of PDI placement provided by origami attenuated coupling and orbital overlap with only a few nt spacings, and became negligible

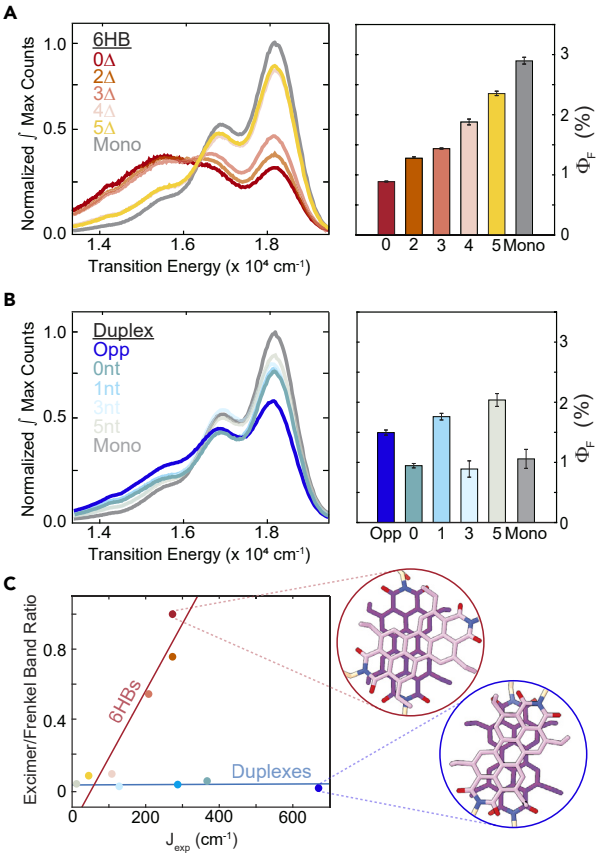


**Figure 3. Steady-state characterization**

(A) (Left) Area-normalized emission spectra of PDI-6HBs produce a red-shifted and broader excimer emission at small PDI-PDI distances (smaller Δ). (Right) PDI-6HB photoluminescence quantum efficiency ($\Phi_F$). Error bars are the standard deviation of three replicates. Consistently smaller $\Phi_F$ are observed at smaller PDI separation concomitant with larger symmetry-forbidden excimer-state population.

(B) (Left) In contrast, emission spectra of duplex PDI dimers show negligible excimer emission even at a minimal PDI separation. (Right) PDI-duplex $\Phi_F$ shows less correlation based on PDI separation.

(C) Excimer/Frenkel emission peak height ratio for 6HB and duplex PDI dimers. There is a strong correlation between experimental excitonic coupling ($J_{exp}$) and measured excimer emission in 6HB dimers, with enhanced excimer emission at increasing $J_{exp}$. In contrast, the excimer/Frenkel emission ratio is unchanged with respect to $J_{exp}$ in duplexes. $\lambda_{excit}$ = 465 nm. (Inset) Simulated MD and DFT structures of 6HB and duplex dimers at highest coupling strengths.

in 4Δ-6HB and 5Δ-6HB. However, we anticipate the reduced coupling, while retaining close (<1.5 nm COM) PDI sequence position in 4Δ-6HB, would support energy transfer, as we previously reported with cyanines.[72,135]

In contrast, no excimer emission was observed on duplexes, even with strongly coupled opp- and 0 nt-duplexes (Figure 3B). We speculated that the lack of duplex excimer emission was a result of a more slip-stacked structure, observed in MD and density functional theory (DFT) studies. Further, slip stacking has been implicated in reduced excimer emission in PDIs.[58,98,99] Importantly, these two distinct structures were achieved with the same dye moiety, showing that control between rotated and slip-stacked geometry was specifically enabled by the versatility of PDI-positional control via DNA assembly. Interestingly, we found that photoluminescence quantum yields ($\Phi_F$) of origami structures were programmable and increased with

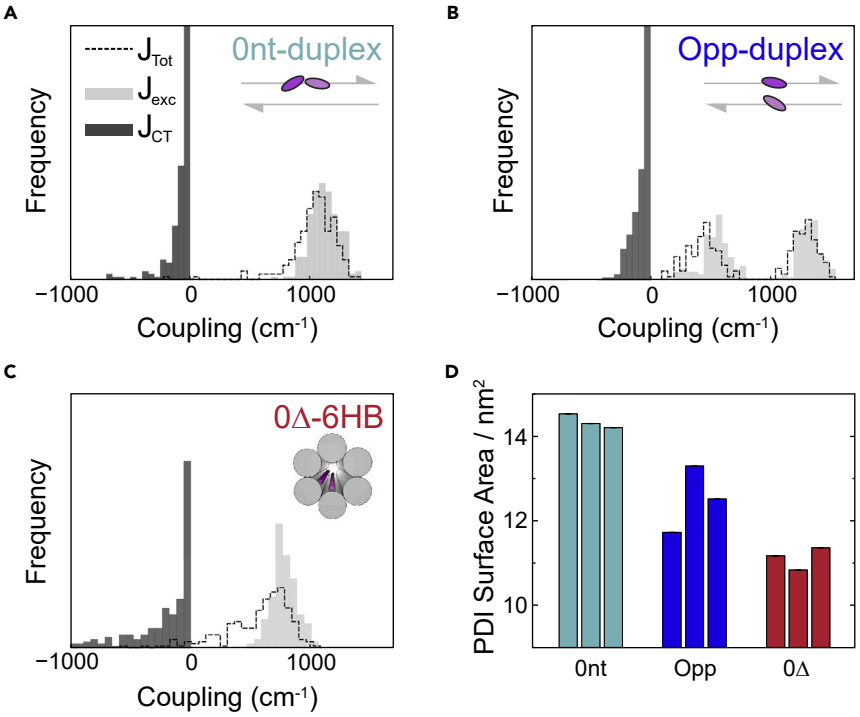


**Figure 4. Structural impact of DNA motifs on dye coupling values**

(A–C) Histograms compiled using DFT calculations on $J_{total}$, $J_{excitonic}$, and $J_{CT}$ performed on the final 2-ns of the MD simulations for (A) 0 nt-duplex, (B) opp-duplex, and (C) 0Δ-6HB all reveal a broad range of couplings. Trends in total coupling strength were well matched to our vibronic lineshapes observed in our absorption spectra analysis.

(D) Solvent-accessible surface areas (SASAs) of PDIs from triplicated MD simulations highlight greater exposure to water in PDI duplexes compared with 0Δ- and 2Δ-6HBs. Error bars were small owing to relatively constant values during the simulation.

dimer spacing in PDI-6HBs (Figure 3A), but not in PDI duplexes (Figure 3B), which further exemplifies the fine control over PDI structure provided by origami. See supplemental information section S7 for further $\Phi_F$ discussion.

To unify our analysis, comparing 6HBs and duplexes for controlling coupling, we quantified the vibronic absorption lineshapes and excimer emission together (Figure 3C). We extracted the experimental coupling values $J_{exp}$ from the vibrational amplitudes of the absorption spectra of the PDIs on 6HBs and duplexes (supplemental information section S8). $J_{exp}$ of 273 $cm^{-1}$ for 0Δ-6HB and 2Δ-6HB were consistent with previously reported values for excimer-generating PDIs.[119] The orbital overlap and dipolar interactions were reduced as PDI separated along the DNA origami, $J_{exp}$ values and excimer populations fell linearly in the 0–5Δ-6HB series. Interestingly, no such correlation was evident in duplexes, despite similar excitonic coupling strengths. This suggests distinct exciton evolution pathways between the excimer-active 6HBs versus duplexes. The lack of spectral shifts, despite strong coupling in PDI duplexes, hinted at SBCT photoproduct formation.

To parse the impact of Coulombic and CT coupling individually and gain a clearer picture of the structural effects of slip-stacked and rotated PDIs in 6HBs and duplexes, we used quantum mechanical (QM) calculations on select MD configurations (Figures 4 and S38–S43). We selected PDI dimer structures for which the calculated total coupling ($J_{total}$) most closely matched the trends observed experimentally, $J_{exp}$

in Figures 2C and 2F. These spectra were fit to well-established theoretical models for PDI vibronic band ratios.[118] We proceeded with the MD replicates that best represented the excitonic couplings observed in our steady-state spectra in Figures 2A and 2B, but the breadth of these structures clearly alluded to significant heterogeneity in the simulated systems. The most strongly coupled structures, opp-duplex, 0 nt-duplex, and 0Δ-6HB, are shown in Figures 4A–4C.

To illustrate the impact of DNA scaffolding on the electronic properties of PDI dimers, we calculated the distribution of both Coulombic ($J_{exc}$) and CT ($J_{CT}$) coupling. Given that multilayer origami structures consist of multiple interconnected duplexes that impart both mechanical rigidity and additional molecular DNA surface and volume for dyes to interact with,[136] we anticipated that the 6HB constructs would display less overall heterogeneity in the photoproduct states formed.[137] Because solvent-accessible surface area (SASA) values report on the relative degree of solvent exposure of the dye to water (Figure 4D), we used SASA as a proxy for how conformationally labile the PDIs were as a function of their scaffolding DNA architecture. We observed a lower SASA for the PDIs in the 6HB structures 0Δ-6HB and 2Δ-6HB compared with duplexes (Figure S44) because they were, on average, associated more tightly with the DNA origami surface and positioned between two neighboring helices. In contrast, PDIs in duplexes protruded out from the DNA structure, with greater solvent exposure, indicating that the duplexes could not easily accommodate their large steric bulk. However, the broad heterogeneity observed in the DFT results of PDI-6HB dimers was inconsistent with the reduced conformational dynamics of the dyes that was introduced by their scaffolding on DNA origami. We speculate the static disorder observed in the simulations of opp-duplex and 2Δ-6HB constructs might originate from local sequence sterics more than time-dependent nanoscale fluctuations of the molecular environment, and therefore has substantial impact on the time-resolved spectroscopic analysis. Turning our attention to CT interactions, we note that CT states are stabilized in high-dielectric constant solvents such as water. The lower SASAs of the PDI aggregates in the 6HBs than in the duplexes were likely to significantly impact product state formation between CT and other product states, requiring pump-probe spectroscopy for quantification of these effects.

## Femtosecond excimer and CT state formation

Having clearly established the formation of excimers in rotated PDIs on DNA origami, we turned to femtosecond transient absorption (fs-TA) spectroscopy to track the temporal evolution of excitonic states capable of identifying dark SBCT states in our structures. First, we analyzed the photoexcited mono-duplex control. The ground-state bleach and stimulated emission (GSB and SE) signatures were reflective of the vibronic progression of PDI, and broad excited-state absorption (ESA) corresponded to the $S_1$-$S_N$ transition 13,750–15,600 $cm^{-1}$ (Figure S45), which decayed on a ~30-ps timescale. We assigned this process to hole transfer from electron-donating purine bases (adenine or guanine) to the electron-withdrawing PDI dye, based on previous reports.[105,138] We expect that this process produced an intermediate radical pair after transfer, where a radical anion sits on the PDI and a cation on a purine. However, the PDI radical ESA peak was outside of our detection range. Furthermore, the PDI is a strong electron acceptor,[139] which can form low energy singlet CT states that couple strongly to the ground state, accelerating recombination.[138] Hence, we and others[105,127,140] observed rapid CT decay and did not detect the radical pair spectrum. To confirm this assignment, we undertook control experiments. We synthesized a purine-free (thymine-only) PDI-ssDNA sequence where hole transfer is thermodynamically disfavored. For this sequence, the single

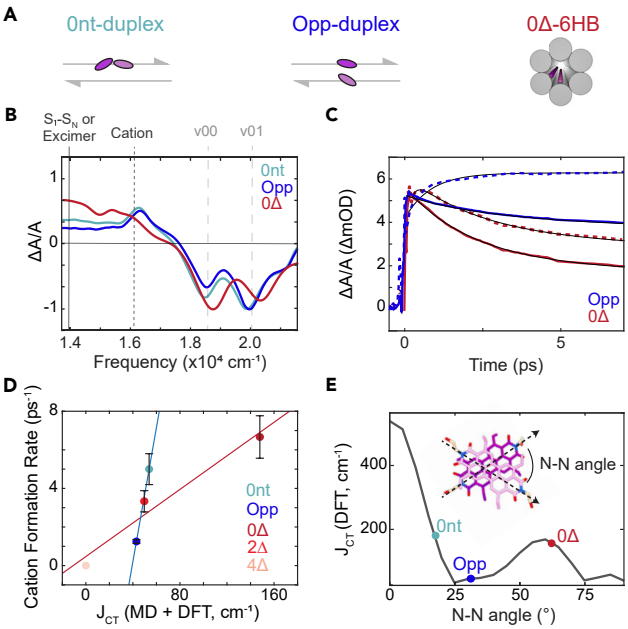


**Figure 5. Dynamics of symmetry-breaking CT (SBCT) and excimer formation**

(A) DNA construct design.

(B) Transient absorption spectra ($\tau$ = 3 ps) for duplex and 6HB-bound dimers.

(C) Opp-duplex-bound dimer and 0Δ-6HB-bound dimer SBCT rise kinetics extracted from decay-associated spectra (DAS). Cation band (dashed) and $S_1$-$S_N$ or excimer band (solid).

(D) Recovered timescales of cation formation plotted against DFT calculated $J_{CT}$ for duplexes and 6HBs from MD simulations (error bars are the standard deviation of three replicates from transient abosrption experiments).

(E) DFT-calculated CT coupling as a function of rotation between geometry-optimized PDI dimers constrained to a 4-Å vertical separation. Representative structures are highlighted.

excited state did not decay by CT (Figures S46–S49), and our DNA-free PDI and the thymine-only control gave near-identical singlet exciton decay rates. These results were consistent with a purine-dependent hole-transfer process in the mono-duplex.

The strong excitonic coupling and slip stacking had suggested that SBCT may be active dimers structured in opp- and 0 nt-duplex (Figures 5A and 5B). GSB and SE features were characteristic of coupled dimer vibronic progression. However, in addition to the broad low energy $S_1$-$S_N$ transition, the ESA also showed a sharp peak centered at 16,300 $cm^{-1}$. We identified this feature as the PDI radical cation, as has been observed previously.[58,59,61,102] We assigned this formation to SBCT, where the delocalized excited singlet state evolves into a polarized anion-cation pair, despite no initial driving force for separation in group-state energy levels.[59,63] To further confirm this PDI cation assignment, we performed chemical oxidation of a DNA-free PDI dye control by $SbCl_5$ in dichloromethane to generate the radical cation species and observed the same absorptive feature at ~16,300 $cm^{-1}$ (Figure S50). The presence of the early-time cation ESA indicated that exciton quenching by hole transfer (as seen in the mono-duplex) could not be the dominant decay pathway in the opp- and 0 nt-duplexes, which would instead produce exclusively a PDI anion that rapidly decays and not the growing cation feature observed. The PDI anion excited-state absorption features occurred at the red edge of our experimental spectrum and were not observed above the $S_1$-$S_N$ transition in our measurements. The absence of probe intensity at 720 nm aligned with the lower intensity boundary of our optical probe, limiting identification. Additionally, the radical anion

feature in SBCT, as noted in prior reports,[105] was broad and lacked distinct features, making its identification challenging through our spectral or kinetic analysis. Nonetheless, ESA of the cation instead pointed toward delocalization of the excited state over two PDIs, characteristic of an SBCT state.[59]

Interestingly, while we had confirmed excimer formation by emission, in the strongly coupled 0Δ-6HB construct, we observed spectroscopic ESA signatures of both the cation (16,300 $cm^{-1}$) and an enhanced intensity in the 15,500–13,800 $cm^{-1}$ region (Figure 5B). The former feature indicated SBCT-like processes, while we assigned this latter feature to excimer formation, matching the steady-state emission spectra. As we increased interdimer spacing in 2Δ-6HB (Figure S51), the intensity of both the excimer and cation bands decreased, reflecting conversion to more monomer-like product states composed of simply an excited singlet. This trend continued for the 4Δ-6HB (Figure S49), which reverted to near-complete monomer-like transient absorption features, pointing to minimal interdimer coupling. For the distance-dependent 6HB dimer series, the trends in transient features reflected those observed in the steady state, where strongly coupled configurations gave rise to bimolecular product states, namely excimers and SBCT states, while weakly coupled configurations showed monomer-like character. This point further emphasized the degree of spatial control when using DNA origami scaffolds to direct the formation of these varying photophysical states.

SBCT and excimer states can be strongly interrelated.[59] Excimers result from strong coupling between singlet and CT states, while SBCT-producing systems are formed from charge stabilization resulting in an excited state with dominant charge-resonance character. Hence, SBCT-active systems are often found in high polar solvents, like water. We note, excimers have been implicated as an intermediate for SBCT and singlet fission photoproducts.[65,130] Stabilization of CT states in covalent, cofacial,[60] or orthogonal[141] PDI dimers has previously been invoked to rationalize differing exciton evolution as a function of solvents. In low dielectric solvents (e.g., toluene), CT-stabilization and more Frenkel and charge mixing had generated excimers, which was attenuated in high-dielectric solvents (e.g., benzonitrile). Additionally, dielectric effects promoting SBCT have even been found in solid-state PDIs that possess highly polar side chains.[142] Further, accurate thermodynamic analysis of CT-active DNA-dye systems required fitting of the local dielectric constant on DNA that was considerably lower than bulk water.[143,144] In this report, less-exposed (low SASA) PDI-6HBs experienced a lower local environmental polarity around the dyes (see Figures 4D and S44). Further, the solvation shield in our 6HBs and its low-polarity environment may contribute to greater stabilization of the CT state in 0Δ- and 2Δ-6HBs and more mixing between Frenkel and CT states. Taken together, the local, less-polar origami environment plays a role in our observed excimer population in our 6HBs.

To better correlate the relationship between SBCT and excimer states in our systems, we quantified the extent of excimer and CT character using global analysis for the opp-duplex and the 0Δ-6HB dimers. Here, the frequency- and time-dependent spectra (Figures 5B and 5C) were fitted to a two-component parallel model allowing for the extraction of both short-time (15- to 50-ps timescale) and long-time (400- 900-ps timescale) decay-associated spectra (DAS). The observation of both features at early times ($\tau$ = 3 ps) in the spectrum (Figure S51) suggested that the long-time analysis was dominated by independent decay routes, in line with a parallel global model. This analysis excluded the first 2-ps of data to avoid over-parameterizing the global model. For all dimers in both duplexes and 6HBs, the short-time

DAS component reflected a more excimer-like product spectrum with a larger intensity from 15,500 to 13,800 $cm^{-1}$. The long-time component retained greater intensity of the narrow 16,300-$cm^{-1}$ ESA band, indicative of greater CT character. For both the 0- and 2Δ-6HBs, the excimers exhibited a larger relative amplitude at early times than for the duplexes (Figure S51), which were dominated by the cation peak. We speculate that the static disorder of the DNA environment plays a large role in the generation of these different photoproducts, giving rise to the parallel decay in the model. Past reports on DNA-dye duplexes,[72,145,146] tiles,[74,83] and origami[89,147,148] indicated that small sequence changes can influence photoproducts. Although we designed our constructs for consistency in the origami strand crossovers, termini, dye positions, and orientations of the PDI dimers across all 10 repeat units in the 6HBs, achieving identical nt sequences in each repeat unit is infeasible. This limitation arises in part from the requirement that the DNA origami scaffold must be variable along its length, without repetitive sequences, to fold uniquely into a single target shape.[32] Assembled structural subunits are anticipated to differ slightly within each repeat unit due to these sequence differences, as well as subtle variations in twist,[149] and therefore likely contribute at least in part to heterogeneous PDI dimer structures within the same origami. Furthermore, dynamic fluctuations in PDI stacking and their association with the fluctuating DNA environment likely also contribute to the observed heterogeneity. Dynamic heterogeneity in a phosphate-linked PDI, which shares similarities with our work,[150] showed that PDIs slide across one another every 1–2 $ns^{-1}$. However, we speculate that the sterics of the four ethylphosphonate groups in the present constructs may slow these dynamics. Further, dsDNA exhibits dynamic "DNA breathing" motions, exhibiting $\mu$s bp fluctuations,[151,152] which are capable of temporal cyanine dimer separation.[74] However, PDI dimers have considerably higher affinities[153] than cyanines,[154] which may reduce such breathing dynamics in the present work.

The cation rise time (Figure 5C), which corresponds to the rate of SBCT production and scales with strongly coupled dimer configuration, was also extracted from our data. Here, the 0Δ-6HB construct showed the fastest rate of cation formation in a time of 150 fs, while the opp-duplex dimer showed the slowest cation formation time of 800 fs. The lack of inverse correlation between population (from DAS intensity) and cation rise time further suggested that excimer and cation product state formation occurred in parallel for different subpopulations, as they were not competitive processes for deactivation of the initially excited state. Although the excimer band appeared instantaneously with excitation, the cation band grew on the hundreds-of-fs timescale. We did not observe concomitant decay of the excimer or $S_1$-$S_N$ features on this timescale. This finding suggested that the formation of these product states occurred through parallel pathways, according to heterogeneous configurations within the ensemble of DNA scaffolds, and indicates subpopulations of rotated and slipped PDI structures.

To aid in quantifying the functional differences between the coupled dimer assemblies (opp- and 0 nt-duplexes and 0Δ-, 2Δ-, and 4Δ-6HBs), we compared the relative magnitudes of interdye coupling. First, we examined how the cation formation rate scaled as a function of coupling (Figure 5D), inferred from fitting the MD and DFT analyses. In our simulations, increasing coupling in 6HBs correlated strongly with increasing excimer population, while strong duplex coupling remained excimer free. For the 6HB assemblies, the cation formation rate showed a moderate positive correlation to the interdimer coupling. In contrast, the duplex assemblies showed a considerably steeper positive correlation, suggesting that they were in different regimes of driving forces according to the donor-acceptor coupling and solvation

energy, consistent with the diverging excimer and SBCT formation trends in Figure 5C. To quantify the dominant character of each product state for the dimer assemblies, we compared the ratio of cation intensity in the long-time DAS to the excimer intensity in the short-time DAS, shown in Figure S52. Here, we note, the overlapping excimer and $S_1$-$S_N$ ESA bands complicated this quantification. However, the trends shown support the time-resolved and steady-state spectra, where the duplex dimers were dominated by only SBCT character, while the 6HB dimers exhibited both SBCT and excimer formation.

To better illustrate the effect of PDI rotation on electronic coupling, we calculated $J_{CT}$ (Figure 5E) and $J_{exc}$ (Figure S52) for a pair of geometry-optimized PDIs as a simple toy model. We constrained simulations to a 4.0-Å $\pi$-distance and varied rotational angle, defined by the vector spanning the opposing N atoms in the PDI molecule, roughly aligning with the dipole moment vector. The resulting surface shows that short-range $J_{CT}$ was highly sensitive to the molecular packing geometry, as it relied on constructive or destructive interference between frontier molecular orbitals of neighboring molecules. Recent developments have highlighted the importance of CT-induced photophysics in generating excimers, singlet fission, and SBCT products.[60,65,155] Maximal $J_{CT}$ occurred at 0° when PDIs were aligned, as parallel stacking leads to near-perfect frontier molecular orbital overlap between molecules, falling to zero when PDIs were fully orthogonal. Although we observed a consistent decrease of CT coupling up to an angle of ~30°, where destructive interference drives $J_{CT}$ to zero, a local maximum appeared at an offset of ~65°, coinciding with a slight alignment of the aromatic rings. $J_{exc}$ was maximal at 0° rotation (Figure S42) and weakened as the rotation angle was increased, reaching zero when the dyes were stacked orthogonally.

Finally, we compare our simplified toy model as a function of rotation to the coupling distributions from the MD simulations. The representative structures of 0 nt-duplex, opp-duplex, and 0Δ-6HB are highlighted, with angles of 17.6°, 31.1°, and 61.7°, respectively (Figure 5E). The duplex populations generally occupied a smaller rotation angle and therefore the largest $J_{exc}$ across all constructs alongside reasonable CT couplings, and these results are consistent with our identification of the SBCT-active slip-stacked arrangement initially targeted. On the other hand, the 0Δ-6HB dimer was located at a region with smaller $J_{exc}$, but at a local maxima for $J_{CT}$. We speculate that this unexpected CT coupling enhancement may also contribute to the observed SBCT, alongside targeted excimer formation, in our fs-TA experiments.

## DISCUSSION

We sought to program distinct PDI dimer geometries to control their photoproducts within the context of DNA origami. DNA origami offers a versatile dye scaffolding platform that can in principle host hundreds to thousands of dyes, like natural light-harvesting systems, yet with full synthetic control over dye placements to control photoproducts and their functionality. Although previous studies demonstrated DNA-based structural control to generate desired product states for a few dyes,[51,72–75,156,157] they have not yet replicated the function nor scale of natural systems. The 6HB-based DNA origami system reported here provides a step in this direction, offering discrete control over dye separation and geometric rotation, which were, together with systematic structure-based screening, used to realize excimer-active PDI dimers with fine-control over CT coupling in the context of a large-scale DNA-based structural scaffold (Figures 2D and 5E). Specifically, our approach combined the broad chemical toolkit offered by synthetic DNA chemistry with sub-nm

spatial control using DNA origami. The 6HB scaffold also introduced control over solvation that directly impacted the product states, with SBCT having a clear solvation dependence, favored in more-polar, higher-dielectric environments, where exciton states and intermediates with CT character are stabilized.[33] Importantly, this local polarity control could be leveraged in the future to exploit CT coupling needed for singlet fission in PDIs and, more broadly, for other dyes. Taken together, DNA origami offers unique synthetic control over dimer geometry and local solvent environment, in addition to full control over 3D scaffold geometry,[158–162] providing a platform with the ability to select emergent product states for an excitonic system.

Critically, the 6HB structure enabled the construction of photoactive systems on a larger scale than the individual photoactive PDI dimer itself, spatially organizing 20 PDI dyes stably despite the large number of dye substitutions, which would be infeasible with individual duplexes of DNA. High mechanical rigidity of 6HBs, reflected in a persistence length that reaches several micrometers as opposed to ~50 nm for a duplex, endows additional stability to the structure and function of eventual artificial-light-harvesting systems fabricated with this approach.[136] Future work to accommodate hundreds of dyes offers a blueprint toward building functional multi-dye assemblies approaching the size of nature's light-harvesting complexes. Benchmarking this system, LH2 in purple *Rhodobacter sphaeroides* achieves a relatively high dye per protein volume density (0.28 $nm^{-3}$),[163] while our PDI-6HBs yielded a PDI:DNA density of 0.01 $nm^{-3}$. This was in the order of allophycocyanin[164] and peridinin-chlorophyll-proteins[165] (~0.05 $nm^{-3}$) but considerably less than the Fenna-Matthews-Olsen[166] or LH1/2[103] (0.18–0.38 $nm^{-3}$) (Table S15). Although our primary focus was on dimeric systems to control photoproducts, with the ultimate goal of achieving size and control parity between nature's photosystems and our optoelectronic dyes, we anticipate that higher PDI loading can be achieved in the future by functionalizing all six helices to reduce the scale of the 42-nt repeating motif. At present, this report focuses on dimeric interactions that do not require such high packing densities and coupling between many closely packed dyes, but larger aggregates may be targeted in future work. Further, we anticipate that our designer approach and workflow can also be used to build naive DNA-origami-scaffolded libraries that display many non-nucleosidic molecules for high-throughput photophysical optimization.

Our work demonstrated that the programming of origami structures plays a crucial role in determining the ultimate fate of an exciton into CT or excimers, solely based on the local nucleic acid environment and analogous to the structural proteins in photosynthesis. Notably, we show the programmability of these nucleic acid environments to search for specific dye packing geometries that dictate the photoproduct states, and this now establishes design principles for constructing more intricate and multifunctional systems. Specifically, we have replicated the exciton evolution to SBCT observed in nature's special pair for photochemistry, but using PDI molecules typically employed in optoelectronic devices. We have showcased how these photoproducts can be rationally attenuated by dye position within a 5 Δ/nts region (~1.7 nm) on 6HBs. These weakly coupled but close 4Δ-6HB structures may be used to create densely packed PDI arrays, suited instead for optimizing energy transfer in large antennae complexes that funnel into our excimer or CT-active dimers, which are designs challenging to envision with duplexes, polymers, or amphiphiles. The multifaceted photophysics in PDI-6HBs show evident parallels with chlorophyll-protein systems, both being capable of positioning a limited set of dye moieties into distinct structures to program exciton evolution into different states for dilute light collection, exciton transport, and SBCT. To fully achieve this in the context of DNA origami, future work should focus on how to interconnect

these distinct structures into fully functional excitonic circuits that absorb light and create charges on the same 6HB. Future efforts to diversify the repertoire of modified nucleic acids capable of this will be highly beneficial. Although DNA nanostructures boast a simple, programmable assembly, protein and liposomal systems benefit from a suite of 22 proteinogenic amino acids available for building, in contrast with the mere 4 standard nucleobases in DNA. This manifests in a broader range of dielectric and hydrophobic environments in protein-dye assemblies, which further modulates couplings, efficiencies, and photoproduct formation. Integrating modified nucleobases and backbones may be a valuable approach to match amino acid scope. Further, electron-accepting dyes, as highlighted in this study, can engage in hole transfer with G (potentially adenine) nucleobases, competing with exciton evolution. Once more, unnatural base modifications could provide a strategy to mitigate these effects. Existing DNA systems fall short of replicating the complex function of natural photosynthetic systems that convert solar energy through photoredox chemistry. Effectively integrating coupled chemical reactions and directing the transport of their reagents and products poses a substantial design challenge for origami.

### Conclusions

A series of biomimetic DNA nanostructures with multiple conjugated PDI dyes have been synthesized, characterized, and shown to select for either CT or excimer photoproduct states, as a function of DNA design. Significant control of CT coupling was demonstrated through dye placement across a 5-nt PDI dimer distance and drastically altered the fate of exciton evolution. The DNA origami structure was mechanically rigid and capable of supporting multiple dye modifications into the phosphate backbone. These initial demonstrations laid the ground work for the development of artificial light-harvesting systems that could absorb diffuse light with dense arrays of weakly coupled aggregates and convert these excitons into free charges at strongly coupled dimer sites to power photochemical work.

## EXPERIMENTAL PROCEDURES

### Resource availability

#### *Lead contact*

Further information and requests for resources should be directed to and will be fulfilled by the lead contact, Mark Bathe (mark.bathe@mit.edu).

#### *Materials availability*

The materials generated are available from the lead contact upon reasonable request.

#### *Data and code availability*

The 3D cryo-EM density map of the spoke-containing PDI dyes reported in this manuscript has been deposited in the Electron Microscopy Data Bank (EMDB) with entry ID number EMD-43592.

## SUPPLEMENTAL INFORMATION

Supplemental information can be found online at https://doi.org/10.1016/j.chempr.2024.03.007.

## ACKNOWLEDGMENTS

Work by J.G., S.M.H., M.A.C., A.P.W., M.B., and G.S.S.-C. was supported by the US Department of Energy (DOE), Office of Science, Basic Energy Sciences (BES) under

award DE-SC0019998. T.J. acknowledges financial support from the Alexander von Humboldt Foundation through a Feodor-Lynen Research Fellowship, NSF CCF-1956054, and ONR N00014-17-1-2609. M.A.C. acknowledges support from the Molecular Sciences Software Institute (MolSSI) Software Fellowship program. Part of the computational simulations in this manuscript was performed using resources of the National Energy Research Scientific Computing Center (NERSC), a U.S. Department of Energy Office of Science User Facility located at Lawrence Berkeley National Laboratory, operated under contract No. DE-AC02-05CH11231. Cryo-EM specimens were prepared and imaged at the Automated Cryogenic Electron Microscopy Facility in MIT.nano on a Talos Arctica microscope, which was a gift from the Arnold and Mabel Beckman Foundation. J.G. thanks Xin Luo, Grant Knappe, and Floris Engelhardt for their helpful discussions on origami design, Floris Engelhardt and Benjamin Clancy for scaffold production, and Chi Chen for TEM support. This work was supported in part by the Koch Institute Support (core) grant P30-CA14051 from the National Cancer Institute and the National Institute of Environmental Health Sciences of the NIH under (core) grant P30-ES002109.

## AUTHOR CONTRIBUTIONS

Conceptualization, J.G., S.M.H., M.B., G.S.S.-C., and A.P.W.; formal analysis, T.J., M.A.C., D.H., and J.L.B.; investigation, J.G., S.M.H., T.J., M.A.C., D.H., and M.F.P.; resources, J.G.; software T.J., M.A.C., and D.H.; writing – original draft, J.G., S.M.H., T.J., M.A.C., J.L.B., M.F.P., D.H., M.B., and G.S.S.-C; writing – review and editing, J.G., S.M.H., T.J., M.A.C., D.H., M.F.P., J.L.B., A.P.W., G.S.S.-C., and M.B.; funding acquisition, A.P.W., G.S.S.-C., and M.B.; supervision A.P.W., G.S.S.-C., and M.B.

## DECLARATION OF INTERESTS

The authors declare no competing interests.

Received: November 7, 2023
Revised: February 4, 2024
Accepted: March 11, 2024
Published: April 5, 2024

## REFERENCES

1. Kaskova, Z.M., Dörr, F.A., Petushkov, V.N., Purtov, K.V., Tsarkova, A.S., Rodionova, N.S., Mineev, K.S., Guglya, E.B., Kotlobay, A., Baleeva, N.S., et al. (2017). Mechanism and color modulation of fungal bioluminescence. Sci. Adv. *3*, e1602847. https://doi.org/10.1126/sciadv.1602847.

2. Garcia-Parajo, M.F., Segers-Nolten, G.M.J., Veerman, J.A., Greve, J., and van Hulst, N.F. (2000). Real-time light-driven dynamics of the fluorescence emission in single green fluorescent protein molecules. Proc. Natl. Acad. Sci. USA *97*, 7237–7242. https://doi.org/10.1073/pnas.97.13.7237.

3. Polívka, T., van Stokkum, I.H.M., Zigmantas, D., van Grondelle, R., Sundström, V., and Hiller, R.G. (2006). Energy Transfer in the Major Intrinsic Light-Harvesting Complex from Amphidinium carterae. Biochemistry *45*, 8516–8526. https://doi.org/10.1021/bi060265b.

4. Blankenship, R.E. (2014). Molecular Mechanisms of Photosynthesis (Wiley-Blackwell). https://doi.org/10.1002/9780470758472.

5. Barbatti, M., Aquino, A.J.A., Szymczak, J.J., Nachtigallová, D., Hobza, P., and Lischka, H. (2010). Relaxation mechanisms of UV-photoexcited DNA and RNA nucleobases. Proc. Natl. Acad. Sci. USA *107*, 21453–21458. https://doi.org/10.1073/pnas.1014982107.

6. Schultz, T., Samoylova, E., Radloff, W., Hertel, I.V., Sobolewski, A.L., and Domcke, W. (2004). Efficient Deactivation of a Model Base Pair via Excited-State Hydrogen Transfer. Science *306*, 1765–1768. https://doi.org/10.1126/science.1104038.

7. Steffen, M.A., Lao, K., and Boxer, S.G. (1994). Dielectric Asymmetry in the Photosynthetic Reaction Center. Science *264*, 810–816. https://doi.org/10.1126/science.264.5160.810.

8. Cardona, T., Sedoud, A., Cox, N., and Rutherford, A.W. (2012). Charge separation in Photosystem II: A comparative and evolutionary overview. Biochim. Biophys. Acta *1817*, 26–43. https://doi.org/10.1016/j.bbabio.2011.07.012.

9. Brédas, J.L., Sargent, E.H., and Scholes, G.D. (2016). Photovoltaic concepts inspired by coherence effects in photosynthetic systems. Nat. Mater. *16*, 35–44. https://doi.org/10.1038/nmat4767.

10. Proppe, A.H., Li, Y.C., Aspuru-Guzik, A., Berlinguette, C.P., Chang, C.J., Cogdell, R., Doyle, A.G., Flick, J., Gabor, N.M., van Grondelle, R., et al. (2020). Bioinspiration in light harvesting and catalysis. Nat. Rev. Mater. *5*, 828–846. https://doi.org/10.1038/s41578-020-0222-0.

11. Rosso, C., Filippini, G., and Prato, M. (2021). Use of Perylene Diimides in Synthetic Photochemistry. Eur. J. Org. Chem. *2021*,

1193–1200. https://doi.org/10.1002/ejoc.202001616.

12. Chen, M., Ghiggino, K.P., Launikonis, A., Mau, A.W.H., Rizzardo, E., Sasse, W.H.F., Thang, S.H., and Wilson, G.J. (2003). RAFT synthesis of linear and star-shaped light harvesting polymers using di- and hexafunctional ruthenium polypyridine reagents. J. Mater. Chem. *13*, 2696–2700. https://doi.org/10.1039/B303576J.

13. Xu, L., Wang, Z., Wang, R., Wang, L., He, X., Jiang, H., Tang, H., Cao, D., and Tang, B.Z. (2020). A Conjugated Polymeric Supramolecular Network with Aggregation-Induced Emission Enhancement: An Efficient Light-Harvesting System with an Ultrahigh Antenna Effect. Angew. Chem. Int. Ed. Engl. *59*, 9908–9913. https://doi.org/10.1002/anie.201907678.

14. Han, Y., Zhang, X., Ge, Z., Gao, Z., Liao, R., and Wang, F. (2022). A bioinspired sequential energy transfer system constructed via supramolecular copolymerization. Nat. Commun. *13*, 3546. https://doi.org/10.1038/s41467-022-31094-w.

15. He, G., Yablon, L.M., Parenti, K.R., Fallon, K.J., Campos, L.M., and Sfeir, M.Y. (2022). Quantifying Exciton Transport in Singlet Fission Diblock Copolymers. J. Am. Chem. Soc. *144*, 3269–3278. https://doi.org/10.1021/jacs.1c13456.

16. He, G., Churchill, E.M., Parenti, K.R., Zhang, J., Narayanan, P., Namata, F., Malkoch, M., Congreve, D.N., Cacciuto, A., Sfeir, M.Y., and Campos, L.M. (2023). Promoting multiexciton interactions in singlet fission and triplet fusion upconversion dendrimers. Nat. Commun. *14*, 6080. https://doi.org/10.1038/s41467-023-41818-1.

17. Hüttner, S., Sommer, M., and Thelakkat, M. (2008). n-type organic field effect transistors from perylene bisimide block copolymers and homopolymers. Appl. Phys. Lett. *92*, 93302. https://doi.org/10.1063/1.2885712.

18. Zill, A.T., Licha, K., Haag, R., and Zimmerman, S.C. (2012). Synthesis and properties of fluorescent dyes conjugated to hyperbranched polyglycerols. New J. Chem. *36*, 419–427. https://doi.org/10.1039/C1NJ20476A.

19. Chen, L., Honsho, Y., Seki, S., and Jiang, D. (2010). Light-Harvesting Conjugated Microporous Polymers: Rapid and Highly Efficient Flow of Light Energy with a Porous Polyphenylene Framework as Antenna. J. Am. Chem. Soc. *132*, 6742–6748. https://doi.org/10.1021/ja100327h.

20. Balzani, V., Ceroni, P., Maestri, M., and Vicinelli, V. (2003). Light-harvesting dendrimers. Curr. Opin. Chem. Biol. *7*, 657–665. https://doi.org/10.1016/j.cbpa.2003.10.001.

21. Giansante, C., Raffy, G., Schäfer, C., Rahma, H., Kao, M.T., Olive, A.G.L., and Del Guerzo, A. (2011). White-Light-Emitting Self-Assembled NanoFibers and Their Evidence by Microspectroscopy of Individual Objects. J. Am. Chem. Soc. *133*, 316–325. https://doi.org/10.1021/ja106807u.

22. Jin, X.H., Price, M.B., Finnegan, J.R., Boott, C.E., Richter, J.M., Rao, A., Menke, S.M., Friend, R.H., Whittell, G.R., and Manners, I. (2018). Long-range exciton transport in conjugated polymer nanofibers prepared by seeded growth. Science *360*, 897–900. https://doi.org/10.1126/science.aar8104.

23. Song, Q., Goia, S., Yang, J., Hall, S.C.L., Staniforth, M., Stavros, V.G., and Perrier, S. (2021). Efficient Artificial Light-Harvesting System Based on Supramolecular Peptide Nanotubes in Water. J. Am. Chem. Soc. *143*, 382–389. https://doi.org/10.1021/jacs.0c11060.

24. Vybornyi, M., Vyborna, Y., and Häner, R. (2019). DNA-inspired oligomers: from oligophosphates to functional materials. Chem. Soc. Rev. *48*, 4347–4360. https://doi.org/10.1039/C8CS00662H.

25. Röger, C., Miloslavina, Y., Brunner, D., Holzwarth, A.R., and Würthner, F. (2008). Self-Assembled Zinc Chlorin Rod Antennae Powered by Peripheral Light-Harvesting Chromophores. J. Am. Chem. Soc. *130*, 5929–5939. https://doi.org/10.1021/ja710253q.

26. Del Guerzo, A., Olive, A.G.L., Reichwagen, J., Hopf, H., and Desvergne, J.P. (2005). Energy Transfer in Self-Assembled [n]-Acene Fibers Involving ≥100 Donors Per Acceptor. J. Am. Chem. Soc. *127*, 17984–17985. https://doi.org/10.1021/ja0566228.

27. Son, H.J., Jin, S., Patwardhan, S., Wezenberg, S.J., Jeong, N.C., So, M., Wilmer, C.E., Sarjeant, A.A., Schatz, G.C., Snurr, R.Q., et al. (2013). Light-Harvesting and Ultrafast Energy Migration in Porphyrin-Based Metal–Organic Frameworks. J. Am. Chem. Soc. *135*, 862–869. https://doi.org/10.1021/ja310596a.

28. So, M.C., Wiederrecht, G.P., Mondloch, J.E., Hupp, J.T., and Farha, O.K. (2015). Metal–organic framework materials for light-harvesting and energy transfer. Chem. Commun. (Camb) *51*, 3501–3510. https://doi.org/10.1039/C4CC09596K.

29. Miller, R.A., Presley, A.D., and Francis, M.B. (2007). Self-Assembling Light-Harvesting Systems from Synthetically Modified Tobacco Mosaic Virus Coat Proteins. J. Am. Chem. Soc. *129*, 3104–3109. https://doi.org/10.1021/ja063887t.

30. Park, H., Heldman, N., Rebentrost, P., Abbondanza, L., Iagatti, A., Alessi, A., Patrizi, B., Salvalaggio, M., Bussotti, L., Mohseni, M., et al. (2016). Enhanced energy transport in genetically engineered excitonic networks. Nat. Mater. *15*, 211–216. https://doi.org/10.1038/nmat4448.

31. Curti, M., Maffeis, V., Teixeira Alves Duarte, L.G., Shareef, S., Hallado, L.X., Curutchet, C., and Romero, E. (2023). Engineering excitonically coupled dimers in an artificial protein for light harvesting via computational modeling. Protein Sci. *32*, e4579. https://doi.org/10.1002/pro.4579.

32. Rothemund, P.W.K. (2006). Folding DNA to create nanoscale shapes and patterns. Nature *440*, 297–302. https://doi.org/10.1038/nature04586.

33. Seeman, N.C. (1982). Nucleic acid junctions and lattices. J. Theor. Biol. *99*, 237–247. https://doi.org/10.1016/0022-5193(82)90002-9.

34. Mathur, D., Díaz, S.A., Hildebrandt, N., Pensack, R.D., Yurke, B., Biaggne, A., Li, L., Melinger, J.S., Ancona, M.G., Knowlton, W.B., and Medintz, I.L. (2023). Pursuing excitonic energy transfer with programmable DNA-based optical breadboards. Chem. Soc. Rev. *52*, 7848–7948. https://doi.org/10.1039/D0CS00936A.

35. Bösch, C.D., Abay, E., Langenegger, S.M., Nazari, M., Cannizzo, A., Feurer, T., and Häner, R. (2019). DNA-Organized Light-Harvesting Antennae: Energy Transfer in Polyaromatic Stacks Proceeds through Interposed Nucleobase Pairs. Helv. Chim. Acta *102*, e1900148. https://doi.org/10.1002/hlca.201900148.

36. Bousmail, D., Chidchob, P., and Sleiman, H.F. (2018). Cyanine-Mediated DNA Nanofiber Growth with Controlled Dimensionality. J. Am. Chem. Soc. *140*, 9518–9530. https://doi.org/10.1021/jacs.8b04157.

37. Fendt, L.A., Bouamaied, I., Thöni, S., Amiot, N., and Stulz, E. (2007). DNA as supramolecular scaffold for porphyrin arrays on the nanometer scale. J. Am. Chem. Soc. *129*, 15319–15329. https://doi.org/10.1021/ja075711c.

38. Wang, X., Deshmukh, R., Sha, R., Birktoft, J.J., Menon, V., Seeman, N.C., and Canary, J.W. (2022). Orienting an Organic Semiconductor into DNA 3D Arrays by Covalent Bonds. Angew. Chem. Int. Ed. Engl. *61*, e202115155. https://doi.org/10.1002/anie.202115155.

39. Yamana, K., Takei, M., and Nakano, H. (1997). Synthesis of oligonucleotide derivatives containing pyrene labeled glycerol linkers: Enhhanced excimer fluorescence on binding to a complementary DNA sequence. Tetrahedron Lett. *38*, 6051–6054. https://doi.org/10.1016/S0040-4039(97)01358-0.

40. Barclay, M.S. (2021). Rotaxane rings promote oblique packing and extended excited-state lifetimes in DNA-templated squaraine dye aggregates. Commun. Chem. 1–11. https://doi.org/10.1038/s42004-021-00456-8.

41. Meares, A., Susumu, K., Mathur, D., Lee, S.H., Mass, O.A., Lee, J., Pensack, R.D., Yurke, B., Knowlton, W.B., Melinger, J.S., and Medintz, I.L. (2022). Synthesis of Substituted Cy5 Phosphoramidite Derivatives and Their Incorporation into Oligonucleotides Using Automated DNA Synthesis. ACS Omega *7*, 11002–11016. https://doi.org/10.1021/acsomega.1c06921.

42. Jenkins, Y., and Barton, J.K. (1992). A sequence-specific molecular light switch: tethering of an oligonucleotide to a dipyridophenazine complex of ruthenium(II). J. Am. Chem. Soc. *114*, 8736–8738. https://doi.org/10.1021/ja00048a077.

43. Chan, K.M., Xu, W., Kwon, H., Kietrys, A.M., and Kool, E.T. (2017). Luminescent Carbon Dot Mimics Assembled on DNA. J. Am. Chem. Soc. *139*, 13147–13155. https://doi.org/10.1021/jacs.7b07420.

44. Xu, W., Chan, K.M., and Kool, E.T. (2017). Fluorescent nucleobases as tools for studying

DNA and RNA. Nat. Chem. *9*, 1043–1055. https://doi.org/10.1038/nchem.2859.

45. Ikkanda, B.A., Samuel, S.A., and Iverson, B.L. (2014). NDI and DAN DNA: Nucleic Acid-Directed Assembly of NDI and DAN. J. Org. Chem. *79*, 2029–2037. https://doi.org/10.1021/jo402704z.

46. Manchester, J., Bassani, D.M., Duprey, J.L., Giordano, L., Vyle, J.S., Zhao, Z.Y., and Tucker, J.H.R. (2012). Photocontrolled Binding and Binding-Controlled Photochromism within Anthracene-Modified DNA. J. Am. Chem. Soc. *134*, 10791–10794. https://doi.org/10.1021/ja304205m.

47. Kretschy, N., Sack, M., and Somoza, M.M. (2016). Sequence-Dependent Fluorescence of Cy3- and Cy5-Labeled Double-Stranded DNA. Bioconjug. Chem. *27*, 840–848. https://doi.org/10.1021/acs.bioconjchem.6b00053.

48. Dziuba, D., Jurkiewicz, P., Cebecauer, M., Hof, M., and Hocek, M. (2016). A Rotational BODIPY Nucleotide: An Environment-Sensitive Fluorescence-Lifetime Probe for DNA Interactions and Applications in Live-Cell Microscopy. Angew. Chem. Int. Ed. Engl. *55*, 174–178. https://doi.org/10.1002/anie.201507922.

49. Berndl, S., and Wagenknecht, H.A. (2009). Fluorescent Color Readout of DNA Hybridization with Thiazole Orange as an Artificial DNA Base. Angew. Chem. Int. Ed. Engl. *48*, 2418–2421. https://doi.org/10.1002/anie.200805981.

50. Li, S., Langenegger, S.M., and Häner, R. (2013). Control of aggregation-induced emission by DNA hybridization. Chem. Commun. (Camb) *49*, 5835–5837. https://doi.org/10.1039/c3cc42706d.

51. Duncan, K.M., Kellis, D.L., Huff, J.S., Barclay, M.S., Lee, J., Turner, D.B., Davis, P.H., Yurke, B., Knowlton, W.B., and Pensack, R.D. (2022). Symmetry Breaking Charge Transfer in DNA-Templated Perylene Dimer Aggregates. Molecules *27*, 6612. https://doi.org/10.3390/molecules27196612.

52. Winiger, C.B., Langenegger, S.M., Calzaferri, G., and Häner, R. (2015). Formation of Two Homo-chromophoric H-Aggregates in DNA-Assembled Alternating Dye Stacks. Angew. Chem. Int. Ed. Engl. *54*, 3643–3647. https://doi.org/10.1002/anie.201410041.

53. Lorenzo, E.R., Olshansky, J.H., Abia, D.S.D., Krzyaniak, M.D., Young, R.M., and Wasielewski, M.R. (2021). Interaction of Photogenerated Spin Qubit Pairs with a Third Electron Spin in DNA Hairpins. J. Am. Chem. Soc. *143*, 4625–4632. https://doi.org/10.1021/jacs.0c12645.

54. Orsborne, S.R.E., Gorman, J., Weiss, L.R., Sridhar, A., Panjwani, N.A., Divitini, G., Budden, P., Palecek, D., Ryan, S.T.J., Rao, A., et al. (2023). Photogeneration of Spin Quintet Triplet–Triplet Excitations in DNA-Assembled Pentacene Stacks. J. Am. Chem. Soc. *145*, 5431–5438. https://doi.org/10.1021/jacs.2c13743.

55. Adeyemi, O.O., Malinovskii, V.L., Biner, S.M., Calzaferri, G., and Häner, R. (2012). Photon harvesting by excimer-forming multichromophores. Chem. Commun. (Camb) *48*, 9589–9591. https://doi.org/10.1039/C2CC34183B.

56. Chen, B., Huang, Q., Qu, Z., Li, C., Li, Q., Shi, J., Fan, C., Wang, L., Zuo, X., Shen, J., et al. (2021). Probing Transient DNA Conformation Changes with an Intercalative Fluorescent Excimer. Angew. Chem. Int. Ed. Engl. *60*, 6624–6630. https://doi.org/10.1002/anie.202014466.

57. Bartynski, A.N., Gruber, M., Das, S., Rangan, S., Mollinger, S., Trinh, C., Bradforth, S.E., Vandewal, K., Salleo, A., Bartynski, R.A., et al. (2015). Symmetry-Breaking Charge Transfer in a Zinc Chlorodipyrrin Acceptor for High Open Circuit Voltage Organic Photovoltaics. J. Am. Chem. Soc. *137*, 5397–5405. https://doi.org/10.1021/jacs.5b00146.

58. Lin, C., Kim, T., Schultz, J.D., Young, R.M., and Wasielewski, M.R. (2022). Accelerating symmetry-breaking charge separation in a perylenediimide trimer through a vibronically coherent dimer intermediate. Nat. Chem. *14*, 786–793. https://doi.org/10.1038/s41557-022-00927-y.

59. Young, R.M., and Wasielewski, M.R. (2020). Mixed electronic states in molecular dimers: connecting singlet fission, excimer formation, and symmetry-breaking charge transfer. Acc. Chem. Res. *53*, 1957–1968. https://doi.org/10.1021/acs.accounts.0c00397.

60. Hong, Y., Kim, J., Kim, W., Kaufmann, C., Kim, H., Würthner, F., and Kim, D. (2020). Efficient multiexciton state generation in charge-transfer-coupled perylene bisimide dimers via structural control. J. Am. Chem. Soc. *142*, 7845–7857. https://doi.org/10.1021/jacs.0c00870.

61. Coleman, A.F., Chen, M., Zhou, J., Shin, J.Y., Wu, Y., Young, R.M., and Wasielewski, M.R. (2020). Reversible symmetry-breaking charge separation in a series of perylenediimide cyclophanes. J. Phys. Chem. C *124*, 10408–10419. https://doi.org/10.1021/acs.jpcc.0c02382.

62. Li, H., and Wenger, O.S. (2022). Photophysics of perylene diimide dianions and their application in photoredox catalysis. Angew. Chem. Int. Ed. Engl. *61*, e202110491. https://doi.org/10.1002/anie.202110491.

63. Alzola, J.M., Tcyrulnikov, N.A., Brown, P.J., Marks, T.J., Wasielewski, M.R., and Young, R.M. (2021). Symmetry-Breaking Charge Separation in Phenylene-Bridged Perylenediimide Dimers. J. Phys. Chem. A *125*, 7633–7643. https://doi.org/10.1021/acs.jpca.1c05100.

64. Hippius, C., Schlosser, F., Vysotsky, M.O., Böhmer, V., and Würthner, F. (2006). Energy Transfer in Calixarene-Based Cofacial-Positioned Perylene Bisimide Arrays. J. Am. Chem. Soc. *128*, 3870–3871. https://doi.org/10.1021/ja058007+.

65. Hong, Y., Rudolf, M., Kim, M., Kim, J., Schembri, T., Krause, A.M., Shoyama, K., Bialas, D., Röhr, M.I.S., Joo, T., et al. (2022). Steering the multiexciton generation in slip-stacked perylene dye array via exciton coupling. Nat. Commun. *13*, 4488. https://doi.org/10.1038/s41467-022-31958-1.

66. Stefik, M., Guldin, S., Vignolini, S., Wiesner, U., and Steiner, U. (2015). Block copolymer self-assembly for nanophotonics. Chem. Soc. Rev. *44*, 5076–5091. https://doi.org/10.1039/C4CS00517A.

67. Yablon, L.M., Sanders, S.N., Li, H., Parenti, K.R., Kumarasamy, E., Fallon, K.J., Hore, M.J.A., Cacciuto, A., Sfeir, M.Y., and Campos, L.M. (2019). Persistent Multiexcitons from Polymers with Pendent Pentacenes. J. Am. Chem. Soc. *141*, 9564–9569. https://doi.org/10.1021/jacs.9b02241.

68. Chan, K.M., Kölmel, D.K., Wang, S., and Kool, E.T. (2017). Color-Change Photoswitching of an Alkynylpyrene Excimer Dye. Angew. Chem. Int. Ed. Engl. *56*, 6497–6501. https://doi.org/10.1002/anie.201701235.

69. Jun, Y.W., Wilson, D.L., Kietrys, A.M., Lotsof, E.R., Conlon, S.G., David, S.S., and Kool, E.T. (2020). An Excimer Clamp for Measuring Damaged-Base Excision by the DNA Repair Enzyme NTH1. Angew. Chem. Int. Ed. Engl. *59*, 7450–7455. https://doi.org/10.1002/anie.202001516.

70. Huang, J., Wu, Y., Chen, Y., Zhu, Z., Yang, X., Yang, C.J., Wang, K., and Tan, W. (2011). Pyrene-Excimer Probes Based on the Hybridization Chain Reaction for the Detection of Nucleic Acids in Complex Biological Fluids. Angew. Chem. Int. Ed. Engl. *50*, 401–404. https://doi.org/10.1002/anie.201005375.

71. Conlon, P., Yang, C.J., Wu, Y., Chen, Y., Martinez, K., Kim, Y., Stevens, N., Marti, A.A., Jockusch, S., Turro, N.J., and Tan, W. (2008). Pyrene Excimer Signaling Molecular Beacons for Probing Nucleic Acids. J. Am. Chem. Soc. *130*, 336–342. https://doi.org/10.1021/ja076411y.

72. Hart, S.M., Chen, W.J., Banal, J.L., Bricker, W.P., Dodin, A., Markova, L., Vyborna, Y., Willard, A.P., Häner, R., Bathe, M., et al. (2021). Engineering couplings for exciton excimertransport using synthetic DNA scaffolds. Chem *7*, 752–773. https://doi.org/10.1016/j.chempr.2020.12.020.

73. Hart, S.M., Banal, J.L., Castellanos, M.A., Markova, L., Vyborna, Y., Gorman, J., Häner, R., Willard, A.P., Bathe, M., et al. (2022). Activating charge-transfer state formation in strongly-coupled dimers using DNA scaffolds. Chem. Sci. *7*, 752–773.

74. Huff, J.S., Turner, D.B., Mass, O.A., Patten, L.K., Wilson, C.K., Roy, S.K., Barclay, M.S., Yurke, B., Knowlton, W.B., Davis, P.H., and Pensack, R.D. (2021). Excited-State Lifetimes of DNA-Templated Cyanine Dimer, Trimer, and Tetramer Aggregates: The Role of Exciton Delocalization, Dye Separation, and DNA Heterogeneity. J. Phys. Chem. B *125*, 10240–10259. https://doi.org/10.1021/acs.jpcb.1c04517.

75. Huff, J.S., Davis, P.H., Christy, A., Kellis, D.L., Kandadai, N., Toa, Z.S.D., Scholes, G.D., Yurke, B., Knowlton, W.B., and Pensack, R.D. (2019). DNA-Templated Aggregates of Strongly Coupled Cyanine Dyes: Nonradiative Decay Governs Exciton Lifetimes. J. Phys. Chem. Lett. *10*, 2386–2392. https://doi.org/10.1021/acs.jpclett.9b00404.

76. Cannon, B.L., Kellis, D.L., Patten, L.K., Davis, P.H., Lee, J., Graugnard, E., Yurke, B., and Knowlton, W.B. (2017). Coherent Exciton Delocalization in a Two-State DNA-Templated Dye Aggregate System. J. Phys. Chem. A *121*, 6905–6916. https://doi.org/10.1021/acs.jpca.7b04344.

77. Buckhout-White, S., Spillmann, C.M., Algar, W.R., Khachatrian, A., Melinger, J.S., Goldman, E.R., Ancona, M.G., and Medintz, I.L. (2014). Assembling programmable FRET-based photonic networks using designer DNA scaffolds. Nat. Commun. *5*, 5615. https://doi.org/10.1038/ncomms6615.

78. Spillmann, C.M., Buckhout-White, S., Oh, E., Goldman, E.R., Ancona, M.G., and Medintz, I.L. (2014). Extending FRET cascades on linear DNA photonic wires. Chem. Commun. (Camb) *50*, 7246–7249. https://doi.org/10.1039/C4CC01072H.

79. Vyawahare, S., Eyal, S., Mathews, K.D., and Quake, S.R. (2004). Nanometer-scale Fluorescence Resonance Optical Waveguides. Nano Lett. *4*, 1035–1039. https://doi.org/10.1021/nl049660i.

80. Massey, M., Ancona, M.G., Medintz, I.L., and Algar, W.R. (2015). Time-Gated DNA Photonic Wires with Förster Resonance Energy Transfer Cascades Initiated by a Luminescent Terbium Donor. ACS Photonics *2*, 639–652. https://doi.org/10.1021/acsphotonics.5b00052.

81. Klein, W.P., Díaz, S.A., Buckhout-White, S., Melinger, J.S., Cunningham, P.D., Goldman, E.R., Ancona, M.G., Kuang, W., and Medintz, I.L. (2018). Utilizing HomoFRET to Extend DNA-Scaffolded Photonic Networks and Increase Light-Harvesting Capability. Adv. Opt. Mater. *6*, 1–12. https://doi.org/10.1002/adom.201700679.

82. Zhou, X., Mandal, S., Jiang, S., Lin, S., Yang, J., Liu, Y., Whitten, D.G., Woodbury, N.W., and Yan, H. (2019). Efficient Long-Range, Directional Energy Transfer through DNAlated Dye Aggregates. J. Am. Chem. Soc. *141*, 8473–8481. https://doi.org/10.1021/jacs.9b01548.

83. Cannon, B.L., Patten, L.K., Kellis, D.L., Davis, P.H., Lee, J., Graugnard, E., Yurke, B., and Knowlton, W.B. (2018). Large Davydov Splitting and Strong Fluorescence Suppression: An Investigation of Exciton Delocalization in DNA-Templated Holliday Junction Dye Aggregates. J. Phys. Chem. A *122*, 2086–2095. https://doi.org/10.1021/acs.jpca.7b12668.

84. Melinger, J.S., Khachatrian, A., Ancona, M.G., Buckhout-White, S., Goldman, E.R., Spillmann, C.M., Medintz, I.L., and Cunningham, P.D. (2016). FRET from Multiple Pathways in Fluorophore-Labeled DNA. ACS Photonics *3*, 659–669. https://doi.org/10.1021/acsphotonics.6b00006.

85. Dutta, P.K., Varghese, R., Nangreave, J., Lin, S., Yan, H., and Liu, Y. (2011). DNA-Directed Artificial Light-Harvesting Antenna. J. Am. Chem. Soc. *133*, 11985–11993. https://doi.org/10.1021/ja1115138.

86. Woller, J.G., Hannestad, J.K., and Albinsson, B. (2013). Self-Assembled Nanoscale DNA–Porphyrin Complex for Artificial Light Harvesting. J. Am. Chem. Soc. *135*, 2759–2768. https://doi.org/10.1021/ja311828v.

87. Hemmig, E.A., Creatore, C., Wünsch, B., Hecker, L., Mair, P., Parker, M.A., Emmott, S., Tinnefeld, P., Keyser, U.F., and Chin, A.W. (2016). Programming Light-Harvesting Efficiency Using DNA Origami. Nano Lett. *16*, 2369–2374. https://doi.org/10.1021/acs.nanolett.5b05139.

88. Zhou, X., Liu, H., Djutanta, F., Satyabola, D., Jiang, S., Qi, X., Yu, L., Lin, S., Hariadi, R.F., Liu, Y., et al. (2022). DNA-templated programmable excitonic wires for micron-scale exciton transport. Chem *8*, 2442–2459. https://doi.org/10.1016/j.chempr.2022.05.017.

89. Mathur, D., Kim, Y.C., Díaz, S.A., Cunningham, P.D., Rolczynski, B.S., Ancona, M.G., Medintz, I.L., and Melinger, J.S. (2021). Can a DNA Origami Structure Constrain the Position and Orientation of an Attached Dye Molecule? J. Phys. Chem. C *125*, 1509–1522. https://doi.org/10.1021/acs.jpcc.0c09258.

90. Klein, W.P., Rolczynski, B.S., Oliver, S.M., Zadegan, R., Buckhout-White, S., Ancona, M.G., Cunningham, P.D., Melinger, J.S., Vora, P.M., Kuang, W., et al. (2020). DNA Origami Chromophore Scaffold Exploiting HomoFRET Energy Transport to Create Molecular Photonic Wires. ACS Appl. Nano Mater. *3*, 3323–3336. https://doi.org/10.1021/acsanm.0c00038.

91. Mathur, D., Samanta, A., Ancona, M.G., Díaz, S.A., Kim, Y., Melinger, J.S., Goldman, E.R., Sadowski, J.P., Ong, L.L., Yin, P., and Medintz, I.L. (2021). Understanding Förster Resonance Energy Transfer in the Sheet Regime with DNA Brick-Based Dye Networks. ACS Nano *15*, 16452–16468. https://doi.org/10.1021/acsnano.1c05871.

92. Nicoli, F., Barth, A., Bae, W., Neukirchinger, F., Crevenna, A.H., Lamb, D.C., and Liedl, T. (2017). Directional Photonic Wire Mediated by Homo-Förster Resonance Energy Transfer on a DNA Origami Platform. ACS Nano *11*, 11264–11272. https://doi.org/10.1021/acsnano.7b05631.

93. Boulais, É., Sawaya, N.P.D., Veneziano, R., Andreoni, A., Banal, J.L., Kondo, T., Mandal, S., Lin, S., Schlau-Cohen, G.S., Woodbury, N.W., et al. (2018). Programmed coherent coupling in a synthetic DNA-based excitonic circuit. Nat. Mater. *17*, 59–166. https://doi.org/10.1038/nmat5033.

94. Pan, K., Boulais, E., Yang, L., and Bathe, M. (2014). Structure-based model for light-harvesting properties of nucleic acid nanostructures. Nucleic Acids Res. *42*, 2159–2170. https://doi.org/10.1093/nar/gkt1269.

95. Sebastian, E., and Hariharan, M. (2021). Null Exciton-Coupled Chromophoric Dimer Exhibits Symmetry-Breaking Charge Separation. J. Am. Chem. Soc. *143*, 13769–13781. https://doi.org/10.1021/jacs.1c05793.

96. Hong, Y., Schlosser, F., Kim, W., Würthner, F., and Kim, D. (2022). Ultrafast Symmetry-Breaking Charge Separation in a Perylene Bisimide Dimer Enabled by Vibronic Coupling and Breakdown of Adiabaticity. J. Am. Chem. Soc. *144*, 15539–15548. https://doi.org/10.1021/jacs.2c03916.

97. Le, A.K., Bender, J.A., and Roberts, S.T. (2016). Slow Singlet Fission Observed in a Polycrystalline Perylenediimide Thin Film. J. Phys. Chem. Lett. *7*, 4922–4928. https://doi.org/10.1021/acs.jpclett.6b02320.

98. Eaton, S.W., Shoer, L.E., Karlen, S.D., Dyar, S.M., Margulies, E.A., Veldkamp, B.S., Ramanan, C., Hartzler, D.A., Savikhin, S., Marks, T.J., and Wasielewski, M.R. (2013). Singlet exciton fission in polycrystalline thin films of a slip-stacked perylenediimide. J. Am. Chem. Soc. *135*, 14701–14712. https://doi.org/10.1021/ja4053174.

99. Hartnett, P.E., Timalsina, A., Matte, H.S.S.R., Zhou, N., Guo, X., Zhao, W., Facchetti, A., Chang, R.P.H., Hersam, M.C., Wasielewski, M.R., and Marks, T.J. (2014). Slip-Stacked Perylenediimides as an Alternative Strategy for High Efficiency Non-Fullerene Acceptors in Organic Photovoltaics Slip-Stacked Perylenediimides as an Alternative Strategy for High Efficiency Non-Fullerene Acceptors in Organic Photovoltaics. J. Am. Chem. Soc. *136*, 16345–16356. https://doi.org/10.1021/ja508814z.

100. Schubert, A., Settels, V., Liu, W., Würthner, F., Meier, C., Fink, R.F., Schindlbeck, S., Lochbrunner, S., Engels, B., and Engel, V. (2013). Ultrafast exciton self-trapping upon geometry deformation in perylene-based molecular aggregates. J. Phys. Chem. Lett. *4*, 792–796. https://doi.org/10.1021/jz4000752.

101. Sung, J., Nowak-Król, A., Schlosser, F., Fimmel, B., Kim, W., Kim, D., and Würthner, F. (2016). Direct observation of excimer-mediated intramolecular electron transfer in a cofacially-stacked perylene bisimide pair. J. Am. Chem. Soc. *138*, 9029–9032. https://doi.org/10.1021/jacs.6b04591.

102. Hestand, N.J., and Spano, F.C. (2015). Interference between Coulombic and CT-mediated couplings in molecular aggregates: H- to J-aggregate transformation in perylene-based $\pi$-stacks. J. Chem. Phys. *143*, 244707. https://doi.org/10.1063/1.4938012.

103. Swainsbury, D.J.K., Qian, P., Jackson, P.J., Faries, K.M., Niedzwiedzki, D.M., Martin, E.C., Farmer, D.A., Malone, L.A., Thompson, R.F., Ranson, N.A., et al. (2021). Structures of Rhodopseudomonas palustris RC-LH1 complexes with open or closed quinone channels. Sci. Adv. *7*, eabe2631. https://doi.org/10.1126/sciadv.abe2631.

104. Mishra, A.K., Weissman, H., Krieg, E., Votaw, K.A., McCullagh, M., Rybtchinski, B., and Lewis, F.D. (2017). Self-assembly of perylenediimide-single strand DNA conjugates: Employing hydrophobic interactions and DNA base pairing to create a diverse structural space. Chemistry *23*, 10328–10337. https://doi.org/10.1002/chem.201700752.

105. Zeidan, T.A., Carmieli, R., Kelley, R.F., Wilson, T.M., Lewis, F.D., and Wasielewski, M.R. (2008). Charge-transfer and spin dynamics in DNA hairpin conjugates with perylenediimide as a base-pair surrogate. J. Am. Chem. Soc. *130*, 13945–13955. https://doi.org/10.1021/ja803765r.

106. Neelakandan, P.P., Zeidan, T.A., McCullagh, M., Schatz, G.C., Vura-Weis, J., Kim, C.H., Wasielewski, M.R., and Lewis, F.D. (2014).

Ground and excited state electronic spectra of perylenediimide dimers with flexible and rigid geometries in DNA conjugates. Chem. Sci. *5*, 973–981. https://doi.org/10.1039/C3SC52908H.

107. Wagner, C., and Wagenknecht, H.A. (2006). Perylene-3,4:9,10-tetracarboxylic Acid Bisimide Dye as an Artificial DNA Base Surrogate. Org. Lett. *8*, 4191–4194. https://doi.org/10.1021/ol061246x.

108. Bevers, S., Schutte, S., and McLaughlin, L.W. (2000). Naphthalene- and Perylene-Based Linkers for the Stabilization of Hairpin Triplexes. J. Am. Chem. Soc. *122*, 5905–5915. https://doi.org/10.1021/ja0001714.

109. Rahe, N., Rinn, C., and Carell, T. (2003). Development of donor–acceptor modified DNA hairpins for the investigation of charge hopping kinetics in DNA. Chem. Commun. (Camb) *17*, 2119–2121. https://doi.org/10.1039/B307395E.

110. Gorman, J., Orsborne, S.R.E., Sridhar, A., Pandya, R., Budden, P., Ohmann, A., Panjwani, N.A., Liu, Y., Greenfield, J.L., Dowland, S., et al. (2022). Deoxyribonucleic Acid Encoded and Size-Defined π-Stacking of Perylene Diimides. J. Am. Chem. Soc. *144*, 368–376. https://doi.org/10.1021/jacs.1c10241.

111. Battagliarin, G., Davies, M., Mackowiak, S., Li, C., and Müllen, K. (2012). Ortho-Functionalized Perylenediimides for Highly Fluorescent Water-Soluble Dyes. ChemPhysChem *13*, 923–926. https://doi.org/10.1002/cphc.201100833.

112. Hogrefe, R.I., Vaghefi, M.M., Reynolds, M.A., Young, K.M., and Arnold, L.J. (1993). Deprotection of methylphosphonate oligonucleotides using a novel one-pot procedure. Nucleic Acids Res. *21*, 2031–2038. https://doi.org/10.1093/nar/21.9.2031.

113. Seibt, J., Winkler, T., Renziehausen, K., Dehm, V., Würthner, F., Meyer, H.D., and Engel, V. (2009). Vibronic Transitions and Quantum Dynamics in Molecular Oligomers: A Theoretical Analysis with an Application to Aggregates of Perylene Bisimides. J. Phys. Chem. A *113*, 13475–13482. https://doi.org/10.1021/jp904892v.

114. Seibt, J., Marquetand, P., Engel, V., Chen, Z., Dehm, V., and Würthner, F. (2006). On the geometry dependence of molecular dimer spectra with an application to aggregates of perylene bisimide. Chem. Phys. *328*, 354–362. https://doi.org/10.1016/j.chemphys.2006.07.023.

115. Banal, J.L., Soleimaninejad, H., Jradi, F.M., Liu, M., White, J.M., Blakers, A.W., Cooper, M.W., Jones, D.J., Ghiggino, K.P., Marder, S.R., et al. (2016). Energy Migration in Organic Solar Concentrators with a Molecularly Insulated Perylene Diimide. J. Phys. Chem. C *120*, 12952–12958. https://doi.org/10.1021/acs.jpcc.6b04479.

116. Bouquin, N., Malinovskii, V.L., and Häner, R. (2008). Highly efficient quenching of excimer fluorescence by perylene diimide in DNA. Chem. Commun. (Camb) *17*, 1974–1976. https://doi.org/10.1039/B802193G.

117. Kistler, K.A., Pochas, C.M., Yamagata, H., Matsika, S., and Spano, F.C. (2012). Absorption, Circular Dichroism, and Photoluminescence in Perylene Diimide Bichromophores: Polarization-Dependent H- and J-Aggregate Behavior. J. Phys. Chem. B *116*, 77–86. https://doi.org/10.1021/jp208794t.

118. Hestand, N.J., and Spano, F.C. (2017). Molecular Aggregate Photophysics beyond the Kasha Model: Novel Design Principles for Organic Materials. Acc. Chem. Res. *50*, 341–350. https://doi.org/10.1021/acs.accounts.6b00576.

119. Kaufmann, C., Bialas, D., Stolte, M., and Würthner, F. (2018). Discrete π-Stacks of Perylene Bisimide Dyes within Folda-Dimers: Insight into Long- and Short-Range Exciton Coupling. J. Am. Chem. Soc. *140*, 9986–9995. https://doi.org/10.1021/jacs.8b05490.

120. Fink, R.F., Seibt, J., Engel, V., Renz, M., Kaupp, M., Lochbrunner, S., Zhao, H.M., Pfister, J., Würthner, F., and Engels, B. (2008). Exciton trapping in π-conjugated materials: A quantum-chemistry-based protocol applied to perylene bisimide dye aggregates. J. Am. Chem. Soc. *130*, 12858–12859. https://doi.org/10.1021/ja804331b.

121. Oleson, A., Zhu, T., Dunn, I.S., Bialas, D., Bai, Y., Zhang, W., Dai, M., Reichman, D.R., Tempelaar, R., Huang, L., et al. (2019). Perylene Diimide-Based Hj- and hJ-Aggregates: The Prospect of Exciton Band Shape Engineering in Organic Materials. J. Phys. Chem. C *123*, 20567–20578. https://doi.org/10.1021/acs.jpcc.9b04429.

122. Winfree, E., Liu, F., Wenzler, L.A., and Seeman, N.C. (1998). Design and self-assembly of two-dimensional DNA crystals. Nature *394*, 539–544. https://doi.org/10.1038/28998.

123. Mathieu, F., Liao, S., Kopatsch, J., Wang, T., Mao, C., and Seeman, N.C. (2005). Six-helix bundles designed from DNA. Nano Lett. *5*, 661–665. https://doi.org/10.1021/nl050084f.

124. Parsons, M.F., Allan, M.F., Li, S., Shepherd, T.R., Ratanalert, S., Zhang, K., Pullen, K.M., Chiu, W., Rouskin, S., and Bathe, M. (2023). 3D RNA-scaffolded wireframe origami. Nat. Commun. *14*, 382. https://doi.org/10.1038/s41467-023-36156-1.

125. Wagenbauer, K.F., Engelhardt, F.A.S., Stahl, E., Hechtl, V.K., Stömmer, P., Seebacher, F., Meregalli, L., Ketterer, P., Gerling, T., and Dietz, H. (2017). How We Make DNA Origami. ChemBioChem. Chembiochem *18*, 1873–1885. https://doi.org/10.1002/cbic.201700377.

126. Fried, M.G., and Bloomfield, V.A. (1984). DNA gelation in concentrated solutions. Biopolymers *23*, 2141–2155. https://doi.org/10.1002/bip.360231104.

127. Carmieli, R., Zeidan, T.A., Kelley, R.F., Mi, Q., Lewis, F.D., and Wasielewski, M.R. (2009). Excited State, Charge Transfer, and Spin Dynamics in DNA Hairpin Conjugates with Perylenediimide Hairpin Linkers. J. Phys. Chem. A *113*, 4691–4700. https://doi.org/10.1021/jp900230q.

128. Wang, X., Li, S., Jun, H., John, T., Zhang, K., Fowler, H., Doye, J.P.K., Chiu, W., and Bathe, M. (2022). Planar 2D wireframe DNA origami. Sci. Adv. *8*, eabn0039. https://doi.org/10.1126/sciadv.abn0039.

129. Poppleton, E., Romero, R., Mallya, A., Rovigatti, L., and Šulc, P. (2021). OxDNA.org: a public webserver for coarse-grained simulations of DNA and RNA nanostructures. Nucleic Acids Res. *49*, W491–W498. https://doi.org/10.1093/nar/gkab324.

130. Sebastian, E., Sunny, J., and Hariharan, M. (2022). Excimer evolution hampers symmetry-broken charge-separated states. Chem. Sci. *13*, 10824–10835. https://doi.org/10.1039/D2SC04387D.

131. Kim, W., Nowak-Król, A., Hong, Y., Schlosser, F., Würthner, F., and Kim, D. (2019). Solvent-modulated charge-transfer resonance enhancement in the excimer state of a bay-substituted perylene bisimide cyclophane. J. Phys. Chem. Lett. *10*, 1919–1927. https://doi.org/10.1021/acs.jpclett.9b00357.

132. Panda, S.S., Shmilovich, K., Herringer, N.S.M., Marin, N., Ferguson, A.L., and Tovar, J.D. (2021). Computationally Guided Tuning of Peptide-Conjugated Perylene Diimide Self-Assembly. Langmuir *37*, 8594–8606. https://doi.org/10.1021/acs.langmuir.1c01213.

133. Kasha, M., Rawls, H.R., and Ashraf El-Bayoumi, M.A. (1965). The exciton model in molecular spectroscopy. Pure Appl. Chem. *11*, 371–392. https://doi.org/10.1351/pac196511030371.

134. Kasha, M. (1963). Energy Transfer Mechanisms and the Molecular Exciton Model for Molecular Aggregates. Radiat. Res. *20*, 55–70. https://doi.org/10.1351/pac196511030371.

135. Banal, J.L., Kondo, T., Veneziano, R., Bathe, M., and Schlau-Cohen, G.S. (2017). Photophysics of J-Aggregate-Mediated Energy Transfer on DNA. J. Phys. Chem. Lett. *8*, 5827–5833. https://doi.org/10.1021/acs.jpclett.7b01898.

136. Schiffels, D., Liedl, T., and Fygenson, D.K. (2013). Nanoscale Structure and Microscale Stiffness of DNA Nanotubes. ACS Nano *7*, 6700–6710. https://doi.org/10.1021/nn401362p.

137. Sa-Ardyen, P., Vologodskii, A.V., and Seeman, N.C. (2003). The Flexibility of DNA Double Crossover Molecules. Biophys. J. *84*, 3829–3837. https://doi.org/10.1016/S0006-3495(03)75110-8.

138. Lewis, F.D., Zhang, L., Kelley, R.F., McCamant, D., and Wasielewski, M.R. (2007). A perylenedicarboxamide linker for DNA hairpins. Tetrahedron *63*, 3457–3464. https://doi.org/10.1016/j.tet.2006.10.089.

139. Würthner, F., Saha-Möller, C.R., Fimmel, B., Ogi, S., Leowanawat, P., and Schmidt, D. (2016). Perylene Bisimide Dye Assemblies as Archetype Functional Supramolecular Materials. Chem. Rev. *116*, 962–1052. https://doi.org/10.1021/acs.chemrev.5b00188.

140. Kaufmann, C., Kim, W., Nowak-Król, A., Hong, Y., Kim, D., and Würthner, F. (2018). Ultrafast Exciton Delocalization, Localization, and Excimer Formation Dynamics in a Highly Defined Perylene Bisimide Quadruple

π-Stack. J. Am. Chem. Soc. *140*, 4253–4258. https://doi.org/10.1021/jacs.7b11571.

141. Chen, M., Shin, J.Y., Young, R.M., and Wasielewski, M.R. (2020). Tuning the charge transfer character of the multiexciton state in singlet fission. J. Chem. Phys. *153*, 094302. https://doi.org/10.1063/5.0017919.

142. Ramirez, C.E., Chen, S., Powers-Riggs, N.E., Schlesinger, I., Young, R.M., and Wasielewski, M.R. (2020). Symmetry-Breaking Charge Separation in the Solid State: Tetra(phenoxy) perylenediimide Polycrystalline Films. J. Am. Chem. Soc. *142*, 18243–18250. https://doi.org/10.1021/jacs.0c09185.

143. Tavernier, H.L., and Fayer, M.D. (2000). Distance Dependence of Electron Transfer in DNA: The Role of the Reorganization Energy and Free Energy. J. Phys. Chem. B *104*, 11541–11550. https://doi.org/10.1021/jp001362w.

144. Lewis, F.D., Liu, X., Miller, S.E., Hayes, R.T., and Wasielewski, M.R. (2002). Formation and Decay of Localized Contact Radical Ion Pairs in DNA Hairpins. J. Am. Chem. Soc. *124*, 14020–14026. https://doi.org/10.1021/ja027108u.

145. Heussman, D., Kittell, J., von Hippel, P.H., and Marcus, A.H. (2022). Temperature-dependent local conformations and conformational distributions of cyanine dimer labeled single-stranded–double-stranded DNA junctions by 2D fluorescence spectroscopy. J. Chem. Phys. *156*, 045101. https://doi.org/10.1063/5.0076261.

146. Ashwood, B., Jones, M.S., Ferguson, A.L., and Tokmakoff, A. (2023). Disruption of energetic and dynamic base pairing cooperativity in DNA duplexes by an abasic site. Proc. Natl. Acad. Sci. USA *120*, e2219124120. https://doi.org/10.1073/pnas.2219124120.

147. Adamczyk, A.K., Huijben, T.A.P.M., Sison, M., Di Luca, A., Chiarelli, G., Vanni, S., Brasselet, S., Mortensen, K.I., Stefani, F.D., Pilo-Pais, M., and Acuna, G.P. (2022). DNA Self-Assembly of Single Molecules with Deterministic Position and Orientation. ACS Nano *16*, 16924–16931. https://doi.org/10.1021/acsnano.2c06936.

148. Hübner, K., Joshi, H., Aksimentiev, A., Stefani, F.D., Tinnefeld, P., and Acuna, G.P. (2021). Determining the In-Plane Orientation and Binding Mode of Single Fluorescent Dyes in DNA Origami Structures. ACS Nano *15*, 5109–5117. https://doi.org/10.1021/acsnano.0c10259.

149. Kube, M., Kohler, F., Feigl, E., Nagel-Yüksel, B., Willner, E.M., Funke, J.J., Gerling, T., Stömmer, P., Honemann, M.N., Martin, T.G., et al. (2020). Revealing the structures of megadalton-scale DNA complexes with nucleotide resolution. Nat. Commun. *11*, 6229. https://doi.org/10.1038/s41467-020-20020-7.

150. Kumar, M., Provazza, J., and Coker, D.F. (2021). Influence of solution phase environmental heterogeneity and fluctuations on vibronic spectra: perylene diimide molecular chromophore complexes in solution. J. Chem. Phys. *154*, 224109. https://doi.org/10.1063/5.0054377.

151. Maurer, J., Albrecht, C.S., Herbert, P., Heussman, D., Chang, A., von Hippel, P.H., and Marcus, A.H. (2023). Studies of DNA 'Breathing' by Polarization-Sweep Single-Molecule Fluorescence Microscopy of Exciton-Coupled (iCy3)2 Dimer-Labeled DNA Fork Constructs. J. Phys. Chem. B *127*, 10730–10748. https://doi.org/10.1021/acs.jpcb.3c06463.

152. Adendorff, M.R., Tang, G.Q., Millar, D.P., Bathe, M., and Bricker, W.P. (2022). Computational investigation of the impact of core sequence on immobile DNA four-way junction structure and dynamics. Nucleic Acids Res. *50*, 717–730. https://doi.org/10.1093/nar/gkab1246.

153. Chen, Z., Lohr, A., Saha-Möller, C.R., and Würthner, F. (2009). Self-assembled π-stacks of functional dyes in solution: Structural and thermodynamic features. Chem. Soc. Rev. *38*, 564–584. https://doi.org/10.1039/b809359h.

154. West, W., and Pearce, S. (1965). The Dimeric State of Cyanine Dyes. J. Phys. Chem. *69*, 1894–1903. https://doi.org/10.1021/j100890a019.

155. Le, A.K., Bender, J.A., Arias, D.H., Cotton, D.E., Johnson, J.C., and Roberts, S.T. (2018). Singlet Fission Involves an Interplay Between Energetic Driving Force and Electronic Coupling in Perylenediimide Films. J Am Chem Soc. J. Am. Chem. Soc. *140*, 814–826. https://doi.org/10.1021/jacs.7b11888.

156. Wright, N.D., Huff, J.S., Barclay, M.S., Wilson, C.K., Barcenas, G., Duncan, K.M., Ketteridge, M., Obukhova, O.M., Krivoshey, A.I., Tatarets, A.L., et al. (2023). Intramolecular Charge Transfer and Ultrafast Nonradiative Decay in DNA-Tethered Asymmetric Nitro- and Dimethylamino-Substituted Squaraines. J. Phys. Chem. A *127*, 1141–1157. https://doi.org/10.1021/acs.jpca.2c06442.

157. Barclay, M.S., Chowdhury, A.U., Biaggne, A., Huff, J.S., Wright, N.D., Davis, P.H., Li, L., Knowlton, W.B., Yurke, B., Pensack, R.D., and Turner, D.B. (2023). Probing DNA structural heterogeneity by identifying conformational subensembles of a bicovalently bound cyanine dye. J. Chem. Phys. *158*, 035101. https://doi.org/10.1063/5.0131795.

158. Jun, H., Wang, X., Bricker, W.P., and Bathe, M. (2019). Automated sequence design of 2D wireframe DNA origami with honeycomb edges. Nat. Commun. *10*, 5419. https://doi.org/10.1038/s41467-019-13457-y.

159. Jun, H., Zhang, F., Shepherd, T., Ratanalert, S., Qi, X., Yan, H., and Bathe, M. (2019). Autonomously designed free-form 2D DNA origami. Sci. Adv. *5*, eaav0655. https://doi.org/10.1126/sciadv.aav0655.

160. Veneziano, R., Ratanalert, S., Zhang, K., Zhang, F., Yan, H., Chiu, W., and Bathe, M. (2016). Designer nanoscale DNA assemblies programmed from the top down. Science *352*, 1534. https://doi.org/10.1126/science.aaf4388.

161. Jun, H., Shepherd, T.R., Zhang, K., Bricker, W.P., Li, S., Chiu, W., and Bathe, M. (2019). Automated sequence design of 3D polyhedral wireframe DNA origami with honeycomb edges. ACS Nano *13*, 2083–2093. https://doi.org/10.1021/acsnano.8b08671.

162. Jun, H., Wang, X., Parsons, M.F., Bricker, W.P., John, T., Li, S., Jackson, S., Chiu, W., and Bathe, M. (2021). Rapid prototyping of arbitrary 2D and 3D wireframe DNA origami. Nucleic Acids Res. *49*, 10265–10274. https://doi.org/10.1093/nar/gkab762.

163. Qian, P., Swainsbury, D.J.K., Croll, T.I., Castro-Hartmann, P., Divitini, G., Sader, K., and Hunter, C.N. (2021). Cryo-EM Structure of the Rhodobacter sphaeroides Light-Harvesting 2 Complex at 2.1 Å. Biochemistry *60*, 3302–3314. https://doi.org/10.1021/acs.biochem.1c00576.

164. Marx, A., and Adir, N. (2013). Allophycocyanin and phycocyanin crystal structures reveal facets of phycobilisome assembly. Biochim. Biophys. Acta *1827*, 311–318. https://doi.org/10.1016/j.bbabio.2012.11.006.

165. Hofmann, E., Wrench, P.M., Sharples, F.P., Hiller, R.G., Welte, W., and Diederichs, K. (1996). Structural Basis of Light Harvesting by Carotenoids: peridinin-chlorophyll-Protein from Amphidinium carterae. Science *272*, 1788–1791. https://doi.org/10.1126/science.272.5269.1788.

166. Tronrud, D.E., Wen, J., Gay, L., and Blankenship, R.E. (2009). The structural basis for the difference in absorbance spectra for the FMO antenna protein from various green sulfur bacteria. Photosynth. Res. *100*, 79–87. https://doi.org/10.1007/s11120-009-9430-6.